Systems/Circuits

Prediction of Learned Resistance or Helplessness by Hippocampal-Prefrontal Cortical Network Activity during Stress

Danilo Benette Marques*, Rafael Naime Ruggiero*, Lezio Soares Bueno-Junior†, Matheus Teixeira Rossignoli†, and João Pereira Leite

Department of Neuroscience and Behavioral Sciences, Ribeirão Preto Medical School, University of São Paulo, Ribeirão Preto, São Paulo 14049-900, Brazil

The perception of control over a stressful experience may determine its impacts and generate resistance against future stressors. Although the medial prefrontal cortex (PFC) and the hippocampus (HPC) are implicated in the encoding of stressor controllability, the neural dynamics underlying this process are unknown. Here, we recorded HPC and PFC neural activities in male rats during the exposure to controllable, uncontrollable, or no shocks and investigated electrophysiological predictors of escape performance upon exposure to subsequent uncontrollable shocks. We were able to accurately discriminate stressed from nonstressed animals and predict resistant (R) or helpless (H) individuals based on hippocampal-cortical oscillatory dynamics. Remarkably, R animals exhibited an increase in theta power during CS, while H exhibited a decrease. Furthermore, R exhibited higher HPC to PFC θ synchronization during stress. Notably, HPC-PFC θ connectivity in the initial stress exposure showed strong correlations with escape performance evaluated days later. R rats also showed stronger θ coupling to both γ oscillations and neuronal firing in the PFC. Finally, we found that these distinct features of network dynamics collectively formed a pattern that accurately predicted learned resistance and was lacking in H individuals. Our findings suggest that hippocampal-prefrontal network θ activity supports cognitive mechanisms of stress coping, whose impairment may underlie vulnerability to stress-related disorders.

Key words: depression; electrophysiology; hippocampus; prefrontal cortex; resilience; θ oscillations

Significance Statement

The appraisal of adversities as controllable or uncontrollable is key in determining resilience or risk for stress-related disorders. Here, we performed the first electrophysiological investigation during controllable or uncontrollable stress. Pharmacological studies showed that the prefrontal cortex (PFC) and the hippocampus (HPC) encode stressor controllability, and here we identified the neural activity underlying this process. This "neural signature of stressor controllability" accurately predicted resistance to future stressors and was characterized by increased HPC-PFC oscillatory activity in the θ frequency (4–10 Hz). Our findings suggest a new role of frontal θ oscillations in adaptive stress coping, integrating its emotional and cognitive functions. We also endorse the potential of this biomarker to guide neurophysiologically-informed and rhythm-based stimulation therapies for depression.

Received Jan. 19, 2021; revised Nov. 2, 2021; accepted Nov. 4, 2021.

Author contributions: D.B.M. and R.N.R. designed research; D.B.M. and M.T.R. performed research; D.B.M., R.N.R., and L.S.B.-J. analyzed data; D.B.M. and R.N.R. wrote the first draft of the paper; D.B.M., R.N.R., L.S.B.-J., M.T.R., and J.P.L. edited the paper; D.B.M., R.N.R., L.S.B.-J., M.T.R., and J.P.L. wrote the paper.

This work was supported by National Council for Scientific and Technological Development Grants 134102/2013-4 (to D.B.M.) and 423977/2016-4 (to J.P.L.), the Coordination for the Improvement of Higher Education Personnel Grant 88882.328283/2019-01 (to D.B.M.), and São Paulo Research Foundation Grants 2018/02303-4 (to R.N.R.), 2012/06123-4 (to L.S.B.-J.), 2011/04467-5 and 2020/01510-6 (to M.T.R.), and 2016/17882-4 (to J.P.L.). We thank Luis Fernando Luca, Antonio Renato Meirelles e Silva, Renata Caldo Scandiuzzi, and Daniela Ribeiro for technical support. We also thank Cláudia Maria Padovan, Maria Helena Hunziker, Frederico Graeff, and Nuno Sousa for discussions.

L.S.B.-J. current address: University of Michigan Medical School, Ann Arbor, MI 48109-5624.

*D.B.M. and R.N.R. share first co-authorship.

†L.S.B.-J. and M.T.R. contributed equally to this work.

The authors declare no competing financial interests.

Correspondence should be addressed to Rafael Naime Ruggiero at rafaruggiero@usp.br or rafaruggiero@gmail.com.

https://doi.org/10.1523/JNEUROSCI.0128-21.2021

Introduction

The perception of control over a stressful experience is critical to determine its impacts on the individual (Southwick and Charney, 2012; Cathomas et al., 2019). Generalized expectations that adversities are uncontrollable is a common factor underlying most stress-related psychiatric illnesses, such as depression, anxiety, and posttraumatic stress disorder. Conversely, the appraisal of challenging situations as manageable is associated with resilience and positive outcomes (Kalisch et al., 2015; Feder et al., 2019). Similarly, in experimental models, learning that aversive events are controllable or uncontrollable drives the acquisition of long-term resistance or vulnerability against future stressors, respectively (Maier and Seligman, 1976, 2016). Rats exposed to uncontrollable inescapable shocks (IS) exhibit deficient escape learning, a phenomenon known as "learned helplessness" (Seligman and Maier, 1967), which parallels with potentiated anxiety, delayed

fear extinction (Shors et al., 1989; Maier and Watkins, 1998, 2005; Amat et al., 2005, 2010; Baratta et al., 2007), and numerous biological effects that bear translational validity with clinical depression and anxiety disorders (Willner, 1984; Maier and Watkins, 1998; Pryce et al., 2011; Vollmayr and Gass, 2013). In contrast, subjects exposed to equivalent controllable escapable shocks (ES) do not present such alterations, and in addition, become resistant (R) against subsequent IS (Amat et al., 2006; Baratta et al., 2007; Maier, 2015).

Maier and colleagues demonstrated that prefrontal cortex (PFC) inhibition abolishes the protective effects of stressor controllability in a wide range of behavioral and physiological outcomes (Amat et al., 2005, 2006; Maier, 2015). Many reports also show that the hippocampus (HPC) is differentially sensitive to controllable and uncontrollable stress (Shors et al., 1989; Balleine and Curthoys, 1991; Amat et al., 1998), and that intrahippocampal administration of antidepressants prevents the development of helplessness after IS (Joca et al., 2003). Moreover, hippocampal-prefrontal cortical functional connectivity (Thierry et al., 2000; Gordon, 2011) is modulated by both stress and antidepressants, and participates in both emotional and higher-order cognitive processes that are dysfunctional in stress-related disorders (Jay et al., 2004; Godsil et al., 2013). Although it has been well established that PFC and HPC play critical roles in encoding stressor controllability, the neural dynamics underlying this process remain unknown.

Here, we hypothesized that the encoding of stressor controllability and uncontrollability would be associated with distinct patterns of neural activity related to HPC and PFC interaction during stress. To test this hypothesis, we recorded HPC and PFC local field potentials (LFP) and single-unit activity in rats during the exposure to either ES, yoked IS, or no shocks (NS), all of which signaled by identical conditioned stimuli (CSs). Then, we explored electrophysiological predictors of learned resistance or helplessness to subsequent uncontrollable shocks, as determined by later escape performance. We found an unprecedented association between stressor controllability and enhanced HPC-PFC θ power and synchrony, as well as PFC local θ phase coupling to both fast oscillations and neuronal firing during the anticipation of aversive stimuli. We were also able to implement a linear discriminative model that accurately distinguished stressed from nonstressed animals and predicted R individuals based solely on oscillatory dynamics. Our results indicate that PFC θ activity entrained by HPC underlies the encoding of stressor controllability, and the lack of this protective activity may allow the development of helplessness in the face of severe stress.

Materials and Methods

Subjects

Adult male Wistar rats (8–10 weeks old) were single housed singly in bedded cages in a controlled-temperature room (22 ± 2°C) on a 12/12 h light/dark cycle (lights on at 7 A.M.) with *ad libitum* access to food and water. The procedures followed the National Council for the Control of Animal Experimentation guidelines and were approved by the local Committee on Ethics in the Use of Animals (Ribeirão Preto Medical School, University of São Paulo, protocol 156/2014).

Electrode implantation surgery

Animals were anesthetized with ketamine and xylazine (respectively, 50 and 25 mg/kg, i.p., followed by 70 and 35 mg/kg, i.m.). Body temperature was kept constant during the entire procedure by a heating pad (37 ± 1°C).

Chronic head caps consisted of a bilateral pair of eight-channel connectors (Omnetics): seven channels for each PFC, one channel for each HPC. Electrode impedance range was 672 ± 28 KΩ (mean ± SEM). PFC electrodes consisted of microwire bundles (7 Teflon-coated tungsten, 50 μm) into both prelimbic areas (ventral: 3.2 mm, anterior: 3.0 mm, lateral: ±0.5 mm; bregma-referenced coordinates; Bueno-Junior et al., 2018). Intermediate HPC areas were each implanted with a monopolar electrode targeted at the CA1 region (ventral: 2.5 mm, posterior: 5.7 mm, lateral: ±4.4 mm; Ruggiero et al., 2018). After implantation and fixation of the electrodes, the HPC electrodes were cut and soldered to the remaining available pins of the eight-channels connectors. In addition to the electrodes, microscrews were fastened into the skull, including a ground reference in the interparietal bone area. Electrodes and screws were then cemented together with acrylic resin. Analgesic, antipyretic, and antibiotic drugs were injected after surgery. Animals were allowed to recover for 8–9 d before stress exposure.

Apparatus

We customized a shuttle box system for simultaneous electrophysiological recording, shock delivery, and behavioral monitoring. The system included a relay switch between the recording cable and the preamplifier (see below, Extracellular recordings). Based on pilot tests, automatically turning off this switch during footshocks (at millisecond precision) was proven necessary to avoid grounding through the recording cable, thus assuring consistency of shock intensity. The behavioral apparatus was located inside a soundproof box, and consisted of a chamber (54-cm length × 50-cm height × 33-cm width) divided in two compartments by a removable wall (1-cm length × 1.5-cm height). Footshocks were delivered through stainless steel bars on the floor (see below, Experimental design). The apparatus contained eight equally spaced infrared beams, four per compartment, to track position and translocation.

Experimental design

All behavioral procedures were performed during the light phase (8 A.M. to 6 P.M.) in a controlled-temperature (22 ± 2°C) dark room (0 lux). On day 1, rats were divided into three groups according to the triadic design of behavioral immunization (modified protocol from Amat et al., 2006). Animals underwent ES, yoked IS, or NS (Fig. 1*A*). ES animals were submitted to 100 trials consisting of a CS (CS^+, LED light, 200 lux, 10-s fixed duration), immediately followed by the unconditioned stimulus (US; footshock, 0.6 mA, 10-s maximum duration, unless terminated by escape behavior). Intertrial intervals were in the range of 40 ± 20 s, randomly. ES animals were allowed to escape by jumping the short wall between compartments. Each animal of the IS group was paired (i.e., yoked) with one of the ES group, such that they were also exposed to CS^+ and footshocks of equivalent intensity and durations matched trial-wise. However, IS animals could not terminate shocks by wall jumping as it would for the ES counterparts. NS animals were exposed only to the CS^-. Thus, CS^+ were paired with shocks (either ES or IS) while CS^- were not. On day 2, both ES and IS animals were exposed to 40 trials of uncontrollable IS of 10-s fixed duration. On day 3 (the test session), resistant or helpless behaviors were determined by evaluating escape performance across 30 trials of ES in the same shuttle box apparatus (adapted from Joca et al., 2003). The wall between compartments was removed in the test session to modify the escape response from jumping to running. Changing the behavioral responses between exposure and test substantiates the generalization of either controllability or helplessness to later stressors in studies investigating differential effects of ES versus IS (Maier and Seligman, 1976; Maier, 2015). Thus, animals could terminate each shock by crossing a single time (i.e., fixed ratio 1) between compartments. Trials where the animal did not perform the escape response during the entire shock duration were considered as failures. Behavioral responses were recorded by an automatized software, and all sessions were video monitored.

To classify R versus H individuals, we used k-means clustering (three clusters) with two behavioral dimensions from the test session: mean latency to escape and total number of failures (Vollmayr and Henn, 2001; Wang et al., 2014). All NS animals were included in the cluster with the best escape performance. ES or IS animals that were clustered together

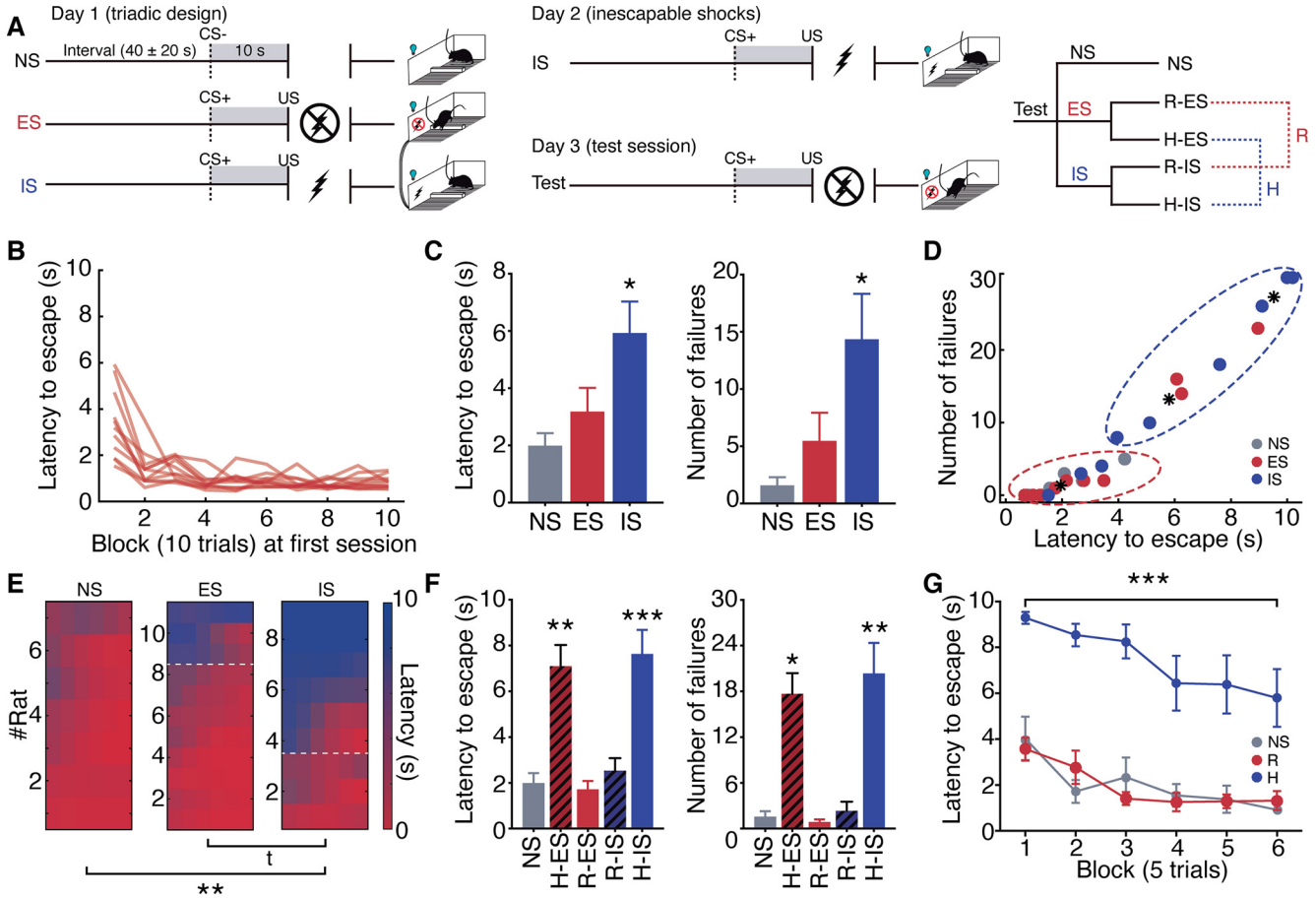

Figure 1. The triadic design of stress exposure induces learned resistance and helplessness. ***A***, Triadic design of stress exposure (day 1) and "immunization" protocol (see Materials and Methods). ***B***, All ES animals learned the escape response at the first exposure. ***C***, IS induced greater mean latency to escape and number of failures in the test session. ***D***, K-means clustering of R and H individuals. ***E***, Latency to escape across blocks. H animals are above the dashed line. IS induced higher proportion of H animals ($^*p < 0.05$, χ^2 test). ***F***, R and H animals exhibited markedly distinct behaviors in the test session. ***G***, R and NS animals showed identical behavior in the test session. H animals exhibited delayed escape learning. Here and on: ES = escapable shocks, IS = inescapable shocks, NS = no shocks, R = resistant, H = helpless, CS = conditioned stimulus (light), US = unconditioned stimulus (shock). $^{\dagger}p < 0.1$, $^*p < 0.05$, $^{**}p < 0.01$, $^{***}p < 0.001$. Error bars represent the mean ± SEM.

with NS were labeled as R, while all others in the poor-performance clusters were labeled as H. Other statistical criteria based on NS behavior, such as the maximum, mean plus two standard deviations, and Tukey's fences outlier range returned the same results, validating our behavioral labeling.

Extracellular recordings

Electrophysiological signals were recorded during behavioral sessions, interrupted only during footshocks (see above, Apparatus). A multichannel acquisition processor (Plexon) was used to record LFPs and multiunit activity (MUA) with the following parameters. LFP: 1000× gain, 0.7- to 500-Hz bandpass filter, 1-kHz sampling rate. MUA: 1000× gain, 150- to 8000-Hz bandpass filter, 40-kHz sampling rate. Timestamps were acquired from the behavioral apparatus at 40-kHz sampling for peristimulus analyses.

Histology

Immediately after the test session, animals were euthanized with CO_2 asphyxiation, and electrolytic lesion currents (1 mA) were applied between pairs of wires. After decapitation, each brain was placed in a cassette for immersion in 4% paraformaldehyde (PFA) overnight (−20° C), followed by 70% ethanol, and paraffin for coronal sectioning at the microtome. Standard cresyl-violet staining was used to validate electrode positioning under the bright-field microscope. Based on histology, we excluded one animal from all analyses, and one animal from HPC analysis. Other five animals were excluded because of electrical noise or excessive locomotion.

Data analysis

Signal processing and analysis of electrophysiological data were performed using custom scripts in MATLAB.

LFPs

LFP were epoched in two peristimulus windows: 8 s around CS onset (4 s pre-CS, 4 s post-CS onset), or 24-s periods encompassing CS and US (8 s pre-CS, 8 s during CS, 8 s after US). Post-US epochs, more specifically, always started 2 s after US offset. Signals were bandpass filtered (1–250 Hz), and epochs with locomotion were excluded based on power spectrum saturation and video inspection. Only epochs when animals expressed immobility were considered while excluding translocation (i.e., active avoidance attempts), pronounced head movements, rearing, and grooming. We chose to investigate locomotion-free epochs because some particular oscillatory activities are correlated with movement, representing a potential confounding factor in our results (Whishaw and Vanderwolf, 1973). Remaining epochs were then subtracted by the averaged epoch. Frequency bands were determined as δ (1–4 Hz), θ (5–10 Hz), α/β (10–30 Hz), low γ (30–50 Hz), and high γ (80–110 Hz). For θ bandpass filtering we used a broader band of 4–10 Hz (Buzsáki and Draguhn, 2004).

Power spectral density (PSD) was calculated using Welch's method (1-s Hamming windowing, 90% overlap, 8192 points). Relative PSD was calculated by dividing the mean PSD estimates by the sum of the averaged pre-CS PSD below 50 Hz. We also investigated θ power and peak frequency by concatenating all locomotion-free 1 s time windows with 90% overlap and calculating relative PSD to the sum of averaged pre-CS

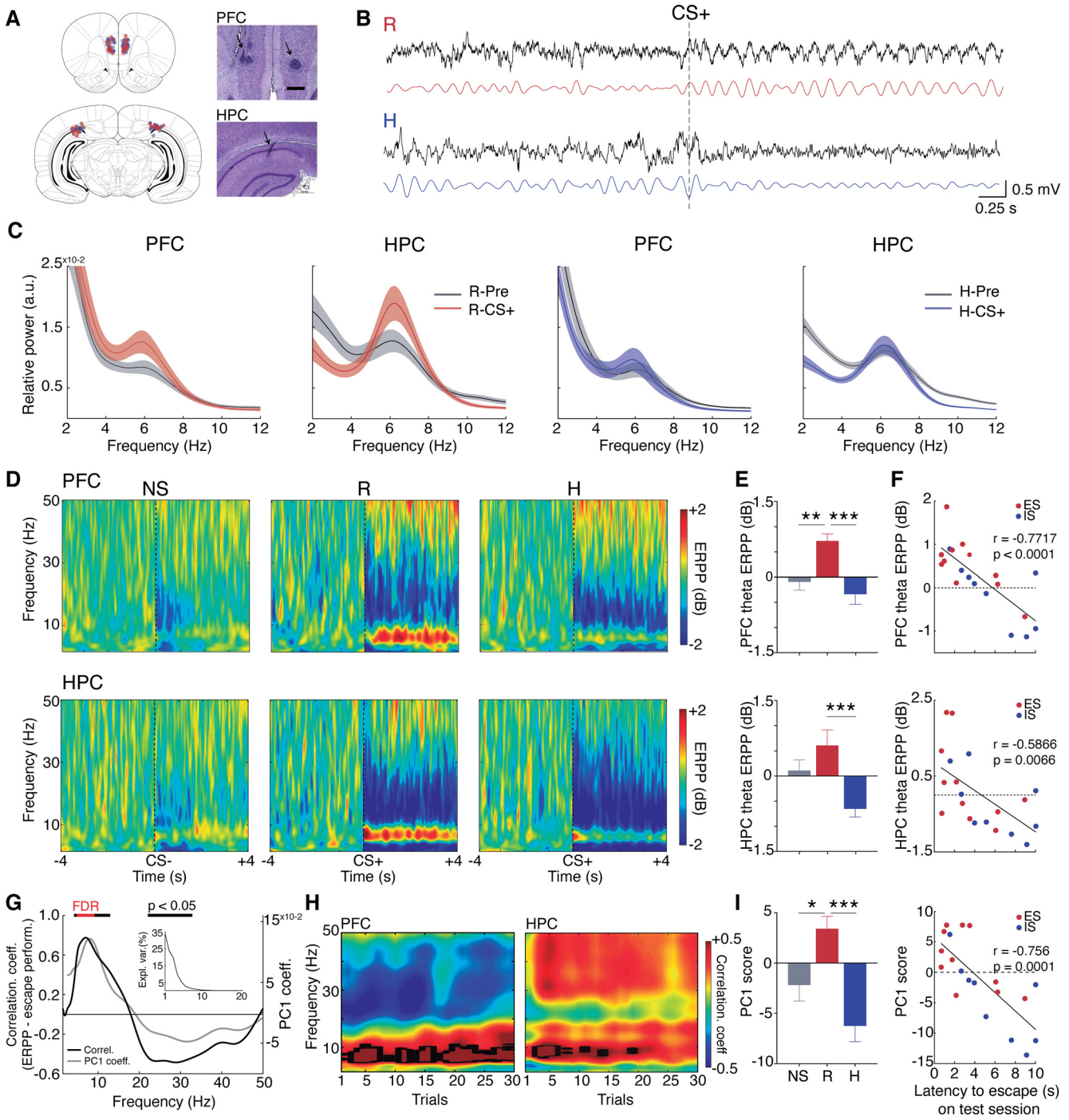

Figure 2. Differential engagement of θ oscillations during the expectation of controllable and uncontrollable stress. ***A***, Electrode placements in the prelimbic area of the PFC and intermediate HPC with representative electrolytic lesions. Gray = NS; red = ES; blue = IS. ***B***, Representative traces of HPC LFPs (black) and θ-filtered signals (colored) preceding controllable (top) and uncontrollable (bottom) shocks. ***C***, PFC and HPC relative PSDs. ***D***, Average spectrograms showing a unique distinction between R and H responses in the θ band. ***E***, Opposite CS^{+}-related modulations of θ power in R (increase) and H (decrease). ***F***, PFC and HPC θ power modulations in the first session correlate with later escape performance. ***G***, The spectrum of correlations between PFC power modulation and escape performance reveals a similar pattern to the PFC power perturbation PC1 coefficients. Black lines = $p < 0.05$, Red line = $p <$ false discovery rate (FDR) corrected. ***H***, PFC presented strong correlations with escape performance throughout the test session. Black lines = $p <$ false discovery rate (FDR) corrected. ***I***, PC1 scores were significantly greater in R animals (left) and showed greater correlation with escape performance than each frequency separately (right); $^{*}p < 0.05$, Fisher's LSD test. Here and on, shaded lines represent the mean ± SEM.

PSD. Normalized PSD was obtained by the ratio in dB (*10*log10*), with the averaged pre-CS PSD for each frequency bin. We detected power peaks within 5–10 Hz per time sample across stimuli. θ Relative and normalized power (dB), and normalized peak frequency (% from the CS period) were compared.

Peristimulus time-frequency decomposition was calculated using complex Morlet wavelet convolution, with 3–20 linearly spaced cycles from 1 to 120 Hz. Full epoch dB single-trial correction was used, and the mean event-related power perturbation (ERPP) was calculated using dB normalization against the pre-CS period, as described in Grandchamp and Delorme (2011). For event-related potentials (ERPs), intertrial coherence (ITC), and phase resetting analyses, data were not subtracted by trial averages. ERP was obtained by averaging LFP across trials. ITC was calculated as the mean resultant length (MRL) of phase differences for each time sample across trials using complex Morlet wavelet (as described above) for frequencies below 30 Hz. For comparisons, we used

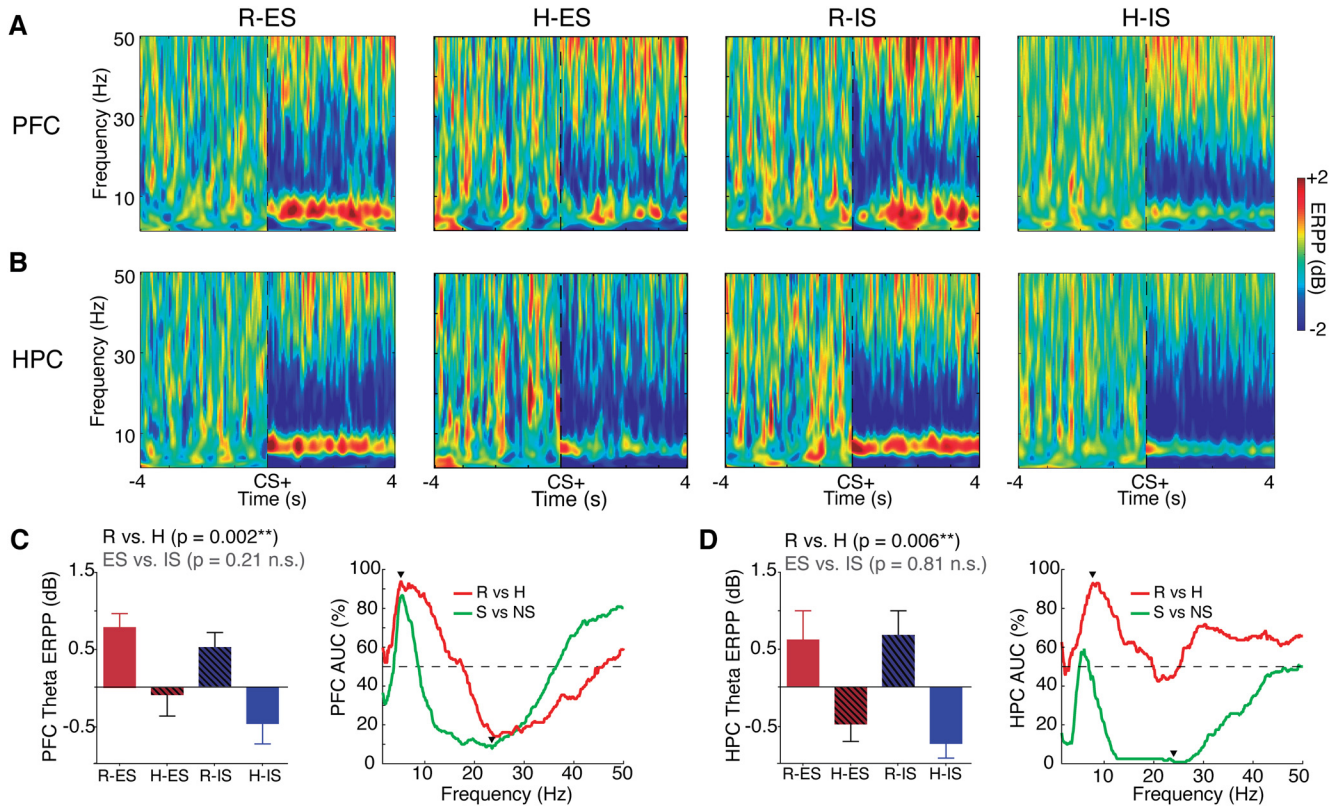

Figure 3. Greater association between PFC and HPC network activities with future behavior (R vs H) than to programmed stress exposure (ES vs IS). ***A***, ***B***, Average spectrograms from all subgroups of (***A***) PFC and (***B***) HPC ERPP. ***C***, ***D***, PFC (***C***) and HPC (***D***) θ ERPP average comparisons (left) and frequency-wise classification performance, estimated by the AUC-ROC (right). Arrows indicate the maximum AUC. Two-way ANOVA significances of behavioral outcome and exposure are reported at the top of panels ***C***, ***D***. S = stressed, n.s. = not significant.

θ ITC in the initial 300 ms after CS onset. For θ phase resetting, we obtained the cosine of the linear interpolation between 0s and πs assigned to the peaks and valleys of the θ bandpass filtered signals (adapted from Courtin et al., 2014). Then we calculated the intertrial variance of these amplitudes. We compared the mean intertrial variance across 0.1-s bins, and in the initial 150 ms after CS onset.

Cross-structural LFP synchrony, an indicative of functional connectivity, was estimated through phase coherence (Lachaux et al., 1999). Spectral mean phase coherence (MPC) was estimated by the MRL of phase differences between signals through Welch's method (same parameters of PSD analysis). Time-frequency decomposition was estimated by the multitaper method using five tapers with time-half bandwidth product of 3, in 1-s segments with 90% overlap. Time-frequency phase coherence perturbation was calculated as described for ERPP. Taking into account the possible nonlinearity of θ oscillations, we also obtained the MRL of the differences between instant phases estimated through Hilbert transform of the θ (4–10 Hz) bandpass filtered signals. For Wiener–Granger causality estimates in the frequency domain, we used the MVGC toolbox (Barnett and Seth, 2014). We used pairs of HPC and PFC LFPs after CS, excluding the initial 300 ms (to avoid nonstationarity of the ERPs). Unfiltered LFP was decimated to 200 Hz, and the model order was estimated by Akaike Information Criterion for each animal separately (model order range: 26–36). We fixed the model order of 36, resulting in an adequate frequency resolution for the slow oscillations predominating in our signals with reasonable computation cost. To estimate the lag between signals, we calculated the cross-correlation of θ bandpass filtered signals and located the time of correlation peaks. With this we obtained both the distribution of lags and average cross-correlation coefficients.

Cross-frequency phase-amplitude coupling indicates how the phases of slower oscillations modulate the amplitude of fast oscillations (Tort et al., 2008, 2009; Ruggiero et al., 2018). We estimated phase-amplitude coupling strength across pairs of frequencies by computing the modulation index (MI; as described by Tort et al., 2010). Comodulation maps were constructed for frequency band pairs varying: (1) from 1 to 50 Hz (0.5-Hz bins) in steps of 1 Hz for phase modulating; and (2) from 10 to 120 Hz (1-Hz bins) in steps of 5 Hz for amplitude modulated. MI between θ band (4–10 Hz) and high γ band (80–110 Hz) were then obtained for statistical comparisons. We concatenated and used all locomotion-free pre-CS and CS periods (5 s) rather than the entire epochs because we did not see evidence for CS-related MI perturbation.

Single-unit activity

Spikes were sorted semi-automatically (Offline Sorter, Plexon) by using principal component analysis (PCA) of spike waveforms, visualization of basic features (amplitude, rate, interspike intervals), and annotations from presorting observations. Sort quality was estimated by the Davies–Bouldin index (DB; range: 0.07–0.47) and J3 value (range: 0.03–4.46) of the three first principal components. We only included channels/units following the criteria: DB < 0.5; multivariate ANOVA $F > 3$ and $p < 0.05$; Dunn index > 1; isolation distance > 30. Individual neurons recorded by more than one channel were identified via cross-correlation (NeuroExplorer, Nex Technologies), and in such cases, only the spike train with the largest waveforms were included in the analysis. The samples of single units (NS: 21, R-ES: 33, H-IS: 35, H-ES: 7, R-IS: 14) were then analyzed in 30-s peristimulus epochs: 10 s pre-CS, 10 s during CS, and 10 s after US offset (similarly to LFP epoching).

Neurons were labeled as modulated or nonmodulated based on stimulus reactivity through comparing pre-CS spike counts versus during-CS and post-US spike counts via one-tailed paired t tests. Modulated neurons were then classified as excited (higher spike count) or suppressed (lower spike count) by each stimulus (CS or US; Wood et al., 2012; Bueno-Junior et al., 2017, 2018). The p value of this categorization was Bonferroni corrected based on the total number of neurons from all groups ($N = 110$, $p = 0.0004$). Firing rate modulation was estimated for each neuron by Z-score normalization against the pre-CS period in bins of 100 ms. The same bin size was used for peristimulus time histograms.

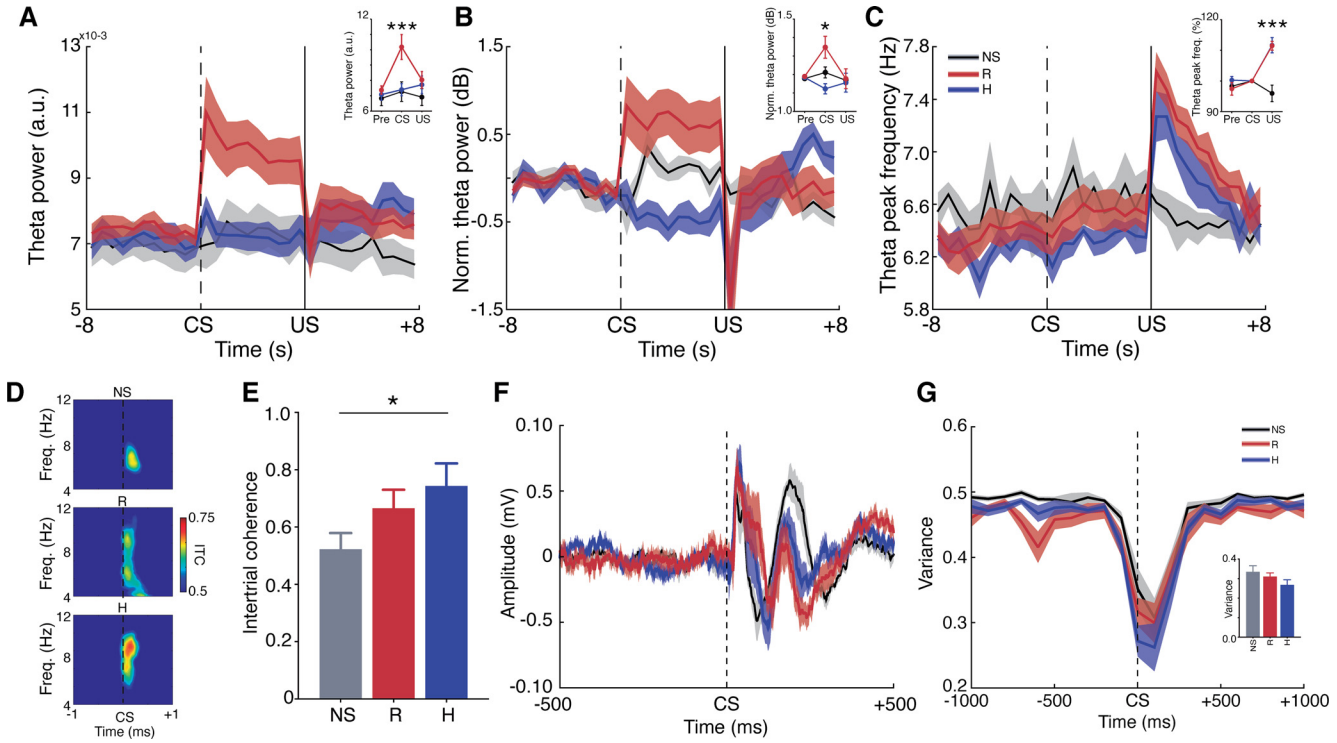

Figure 4. The sustained engagement of θ activity during the anticipation of aversive stimuli is associated with controllability. ***A–C***, Hippocampal θ power and frequency map states of anticipation, reaction, and controllability over aversive stimuli. ***A***, R presented stronger θ power only during CS^+ ***B***, Degree of control over stress bidirectionally influenced θ power modulation during CS^+. ***C***, Increases in θ peak frequency after US were not modulated by the degree of control. Also note that CS^+ did not modulate θ frequency. ***A–C*** insets compare the averages of 4-s periods before CS (pre), after CS onset (CS), and 2 s after shock termination (US). ***D–G***, Greater CS-evoked PFC θ phase resetting in helplessness. ***D***, Average spectrograms of ITC. ***E***, Greater intertrial θ coherence in H than NS in the initial 300 ms. ***F***, Average ERPs were consistent with θ cycles. ***G***, Variance of the standardized θ amplitudes showing a CS-triggered decrease in variance in all groups, especially in helpless animals. Bottom right panel compares mean variances in the initial 150 ms (i.e., one θ cycle). ITC = intertrial coherence; $*p < 0.05$, Fisher's LSD test.

We used the mean Z-score of the initial 1 s after CS onset and initial 1 s after US offset for group comparison.

We then explored more deeply the relationships between CS-evoked and US-evoked responses across neurons. First, all binned Z-scores during CS and post-US (i.e., their entire 10 s) were separately summed up, generating one CS and one US modulation value per neuron. Then, we calculated: (1) net difference as the difference between US and CS values, (2) absolute difference as the modulus of the difference between US and CS values, and (3) relative difference as the difference between the moduli of US and CS values. To identify temporal patterns of neuronal modulation in behavioral categories (stressed, R, and H), we used PCA. PC1 coefficients were obtained from mean Z-scores per bin of all neurons. For each behavioral category, we calculated correlation coefficient moduli between Z-scored firing rate for each neuron and PC1 coefficients. This procedure is based on a previously described method (Chapin and Nicolelis, 1999; Narayanan and Laubach, 2009; Kim et al., 2017), with one adaptation: we replaced the PC1 strength (modulus of the sum of PC1 coefficients projected onto the Z-scored data) by the correlation coefficient, as we observed this coefficient to correspond better to patterns than intensity of modulation.

We also investigated the phase locking of single-unit activity to θ oscillations. Spike times were rounded to the LFP sampling rate (1 kHz), θ phases were assigned to each spike, and their phase locking strength was estimated by pairwise phase consistency (PPC). PPC was calculated as described by Vinck et al. (2010) using the FieldTrip toolbox (Oostenveld et al., 2011). PPC computes the mean of the cosine of the absolute angular distance for all possible pairs of spike phases. This measure is unbiased by the variable number of spikes. Negative values were corrected to zero. The significance of phase-locking was calculated using Rayleigh's Z test (Berens, 2015) with a p value threshold of 0.01, and the Z parameter ($Z = MRL \times \text{number of spikes}^2$) logarithm was computed. Only neurons with >50 spikes during CS in locomotion-free trials were analyzed (as described in Karalis et al., 2016). Spike-triggered average (STA) PSD was determined as the PSD of the averaged LFP across 1-s segments centered at each spike per neuron (adapted from Yang et al., 2018). Firing rhythmicity was assessed by computing spectral estimates on binarized spike data (fire = 1, no fire = 0; similarly to Rosenberg et al., 1989; Royer et al., 2010). Relative STA-PSD, spike PSD, and time-frequency decomposition were computed within 1.5–30 Hz using 1024 points. Windowing parameters were the same as used for LFP analysis.

Multivariate analysis and classification model

To estimate the classification accuracy of behavioral categories by single electrophysiological variables we calculated the area under the receiver operating characteristic curve (AUC-ROC). We explored collective patterns of relationships among electrophysiological data through unsupervised multivariate analysis. Each variable was Z-scored before multivariate analysis, except for power spectra or binned firing rates. PCA was computed using singular value decomposition algorithm, and PC scores were obtained through the projection (i.e., sum of the pointwise multiplication) of PC coefficients onto the original Z-scored data. Common factor analysis was computed using maximum likelihood estimates to obtain factor loadings. Factor scores were in turn obtained by projecting the factor loadings, as described for PCA. Agglomerative hierarchical tree clustering was computed using inner squared Euclidean distance (dissimilarity) and clusters were determined by threshold values of dissimilarity.

To assess the effectiveness of neurophysiological variables to simultaneously classify all stressor controllability-related categories, NS, R, and H, we fitted a regularized linear discriminant classifier model and estimated the classification accuracy. For that, we used the MATLAB function *fitcdiscr* with γ hyperparameter optimization. We deliberately used only two predictors to allow 2D graphical representation and interpretation of model functions. Classification

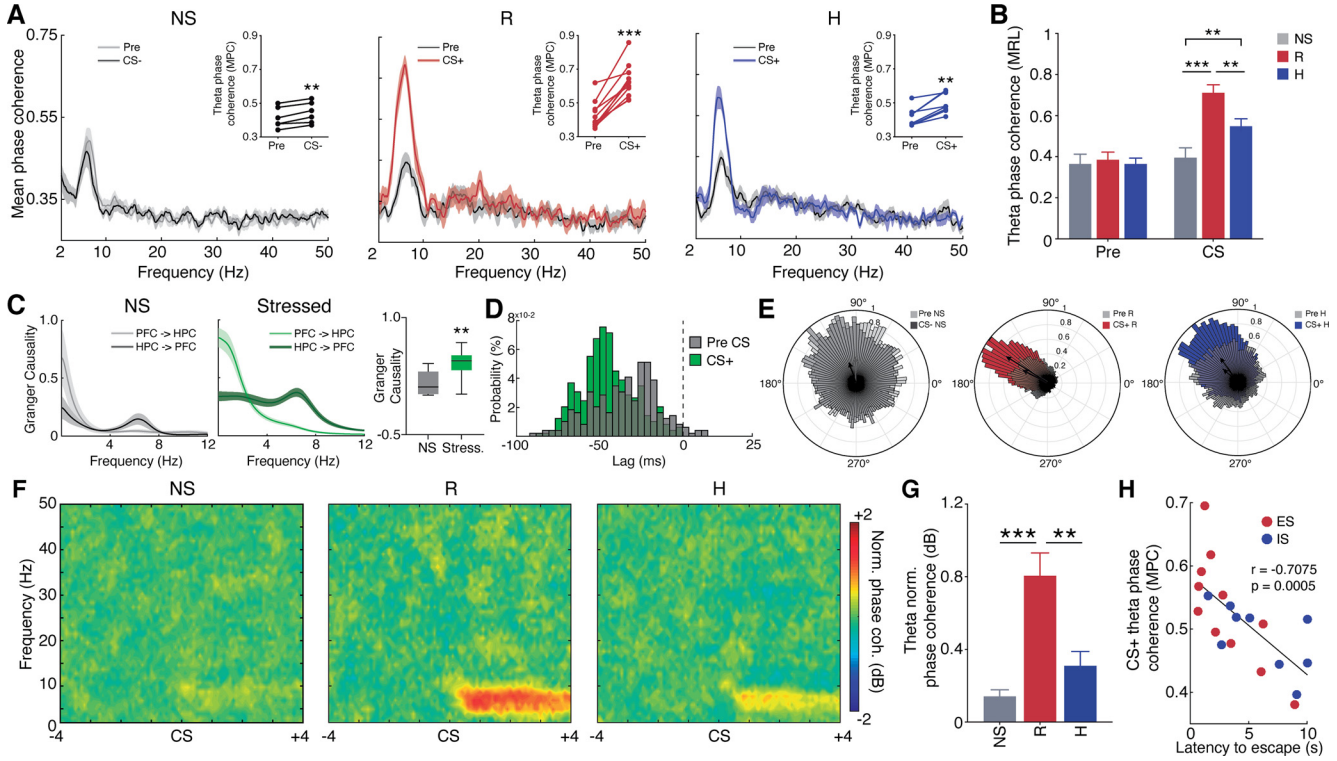

Figure 5. Enhanced HPC to PFC θ synchrony during stress correlates with learned resistance. ***A***, MPC spectra showing a specific modulation of θ band by CS^+. ***B***, Greater θ MRL during CS^+, particularly stronger in R. There were no differences in the pre-CS period. ***C***, Granger causality shows a stronger HPC to PFC θ directionality during CS^+. ***D***, Distribution of lags of cross-correlation coefficient peaks for all trials ($N = 489$). HPC θ consistently preceded (negative values) the PFC in ~49 ms. ***E***, Representative polar histogram of HPC to PFC θ phase differences. Vector sizes indicate the MRL. ***F***, Average spectrograms of event-related phase coherence perturbation. ***G***, R presented significantly greater phase coherence perturbation. ***H***, θ MPC during CS^+ presented a strong correlation with later escape performance.

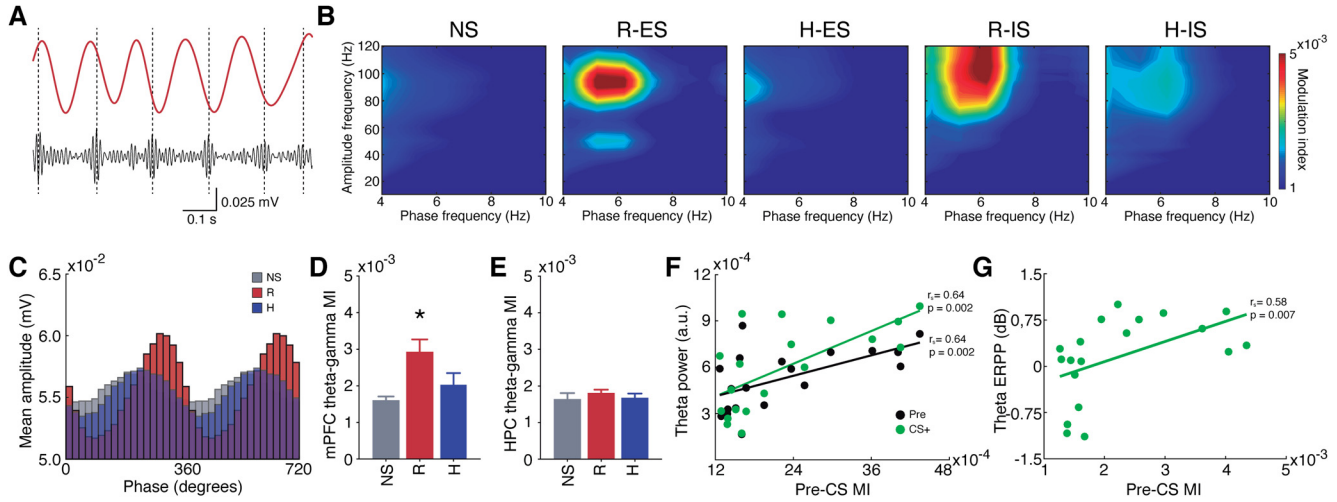

Figure 6. Prestimulus θ-γ phase-amplitude coupling in the PFC is associated with stress resistance and θ power modulation. ***A***, Representative traces of PFC θ (red) and high γ (black) filtered signals. ***B***, PFC phase-amplitude comodulation maps showing blobs of θ-high γ phase-amplitude coupling in R animals from both ES and IS. ***C***, θ phase and high γ amplitude histograms showing stronger coupling in R. ***D***, ***E***, The association between θ-γ coupling and stress resistance was specific to the PFC. ***D***, R presented greater MI than both NS and H. ***F***, ***G***, PFC pre-CS^+ MI showed (***F***) a stronger correlation with CS^+ θ power (green) than pre-CS^+ θ power (black) and (***G***) also correlated with CS^+ θ power perturbation (Spearman's correlation).

accuracy was finally determined as the probability of correct category assignments considering all animals, and then through leave-one-out cross-validation.

Statistical analyses

We used paired *t* tests for within-group comparisons, one-way ANOVA for comparisons between three or more groups, and two-way ANOVA with repeated measures for comparisons across time bins, or periods. We used two-way ANOVA to compare the effects of behavior (R vs H) and stress exposure (ES vs IS) across subsamples. We performed Fisher's least significant difference (LSD) test as *post hoc* analysis after ANOVA. Normality was assessed using the Lilliefors test. When at least one group in a given comparison failed the normality test, we used nonparametric alternatives: Wilcoxon signed-rank test for peristimulus changes, and Kruskal–Wallis test to compare three or more groups, followed by the

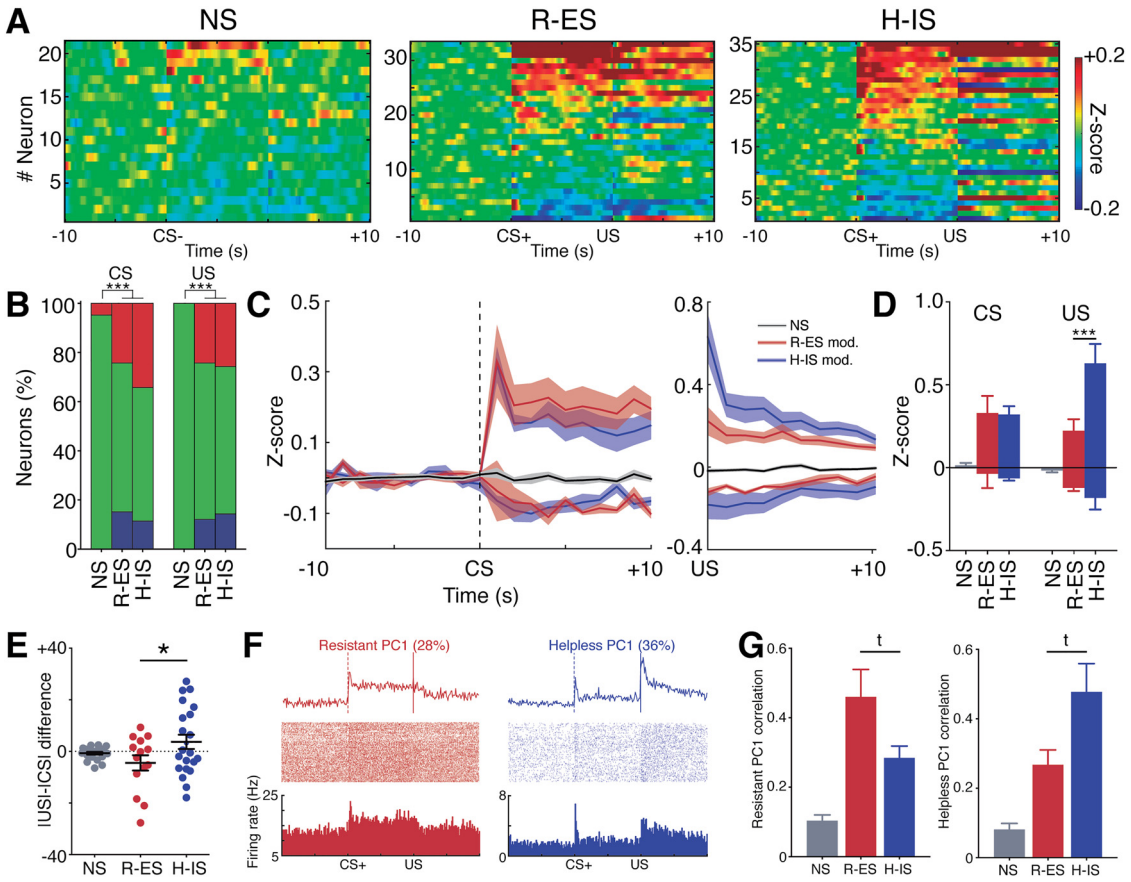

Figure 7. Differential neuronal firing responses to CS^+ and US is associated with controllability or helplessness. ***A***, Firing rate modulation by CS and US. Neurons (*y*-axes) are ordered by CS modulation. There are clear distinctions between NS versus both stressed groups but no clear distinction between R-ES and H-IS. ***B***, Both stressed groups presented more CS-modulated and US-modulated neurons than NS, but no difference was found between R-ES and H-IS. ***C***, ***D***, Firing rate modulation (mean ± SEM) across neuronal categories. ***E***, Bidirectional influence of the degree of control over US-CS differences. R-ES modulated units showed greater responses to CS^+ than US, while H-IS showed the opposite effect. ***F***, PC1 coefficients for all R neurons (left) and H neurons (right) with raster plots from representative neurons corresponding to each pattern. ***G***, Average correlation of modulated neurons with the resistant PC1 and the helpless PC1. $^{\dagger}p < 0.1$.

pairwise Wilcoxon rank-sum *post hoc* test. The χ^2 test was used to compare the proportions of observations (i.e., rats or units) between groups. We calculated Pearson's correlation between normal distributions and Spearman's rank correlation as a nonparametric equivalent. For correlation analysis across trials, we used the false discovery rate correction by the number of trials ($N = 30$). We applied Fisher's Z transform to compare coherence and correlation estimates. Possible outlier subjects were examined using Tukey's fences with three times the lower-to-upper quartile range and, when detected, were excluded from further analysis (one rat was excluded for PFC MI comparisons). Data are expressed as the mean ± SEM. The significance level was set to 0.05 unless stated otherwise. Significances are expressed as $^{\dagger}p < 0.1$, $^{*}p < 0.05$, $^{**}p < 0.01$, and $^{***}p < 0.001$.

Results

Differential engagement of θ oscillations during the expectation of controllable and uncontrollable stress

To identify HPC and PFC neural correlates of stressor controllability and uncontrollability, we submitted rats to controllable ES, uncontrollable IS or NS (Fig. 1*A*; see Materials and Methods). Initially, we confirmed that all ES animals ($N = 11$) learned the escape response on day 1 (Fig. 1*B*). To evaluate whether this initial exposure would generate resistance to future uncontrollable stressors, we exposed both ES and IS animals to IS on day 2 and measured the escape performance of all animals on day 3 (the test session; Fig. 1*A*). Our results show that both the mean latency to escape and the number of failures were equivalent between ES and NS ($N = 7$), but greater in IS ($N = 9$) than ES (latency: one-way ANOVA $F_{(2,24)} = 4.77$, $p = 0.01$; *post hoc* Fisher's LSD test: ES vs NS: $t_{(24)} = 0.95$, $p = 0.36$; ES vs IS: $t_{(24)} = 2.28$, $p = 0.03$; failures: Kruskal–Wallis $H_{(3)} = 7.41$, $p = 0.02$; *post hoc* Wilcoxon rank-sum test: ES vs NS: $U = 33$, $p = 0.62$; ES vs IS: $U = 22$, $p = 0.03$; Fig. 1*C*). This observation confirms the role of controllability in mediating resistance. We then categorized R versus H individuals through cluster analysis based on the similarity with NS behavior (Fig. 1*D*). Previous exposure to ES generated a greater proportion of R individuals (72%, $N = 8/11$) not significantly different from NS [$\chi^2(1, N = 18) = 2.29$, $p = 0.13$], while IS generated a greater proportion of H individuals (66%, $N = 6/9$) significantly different from NS [$\chi^2(1, N = 16) = 7.46$, $p = 0.006$; Fig. 1*E*]. Notoriously, R and H animals showed clearly distinct behavioral profiles in the test session (latency: $F_{(4,22)} = 18$, $p < 0.0001$; number of failures: $H_{(5)} = 18.57$, $p = 0.001$; Fig. 1*F*,*G*). Once we confirmed that the degree of control experienced over stressors was the main factor influencing future escape performance and the emergence of R versus H profiles, we sought to investigate the neural predictors of R and H animals.

We found significant effects of stressor controllability in CS^+ ERPP that were exclusive to the θ band (5–10 Hz) in both PFC ($F_{(2,24)} = 12.23$, $p = 0.0002$; *post hoc*: R vs H: $t_{(24)} = 4.71$, $p < 0.0001$) and HPC ($F_{(2,23)} = 7.80$, $p = 0.002$; *post hoc*: R vs H: $t_{(23)} = 3.94$, $p = 0.0006$; Fig. 2). Moreover, the CS^+ modulations of θ power were the opposite between R and H groups: while R animals

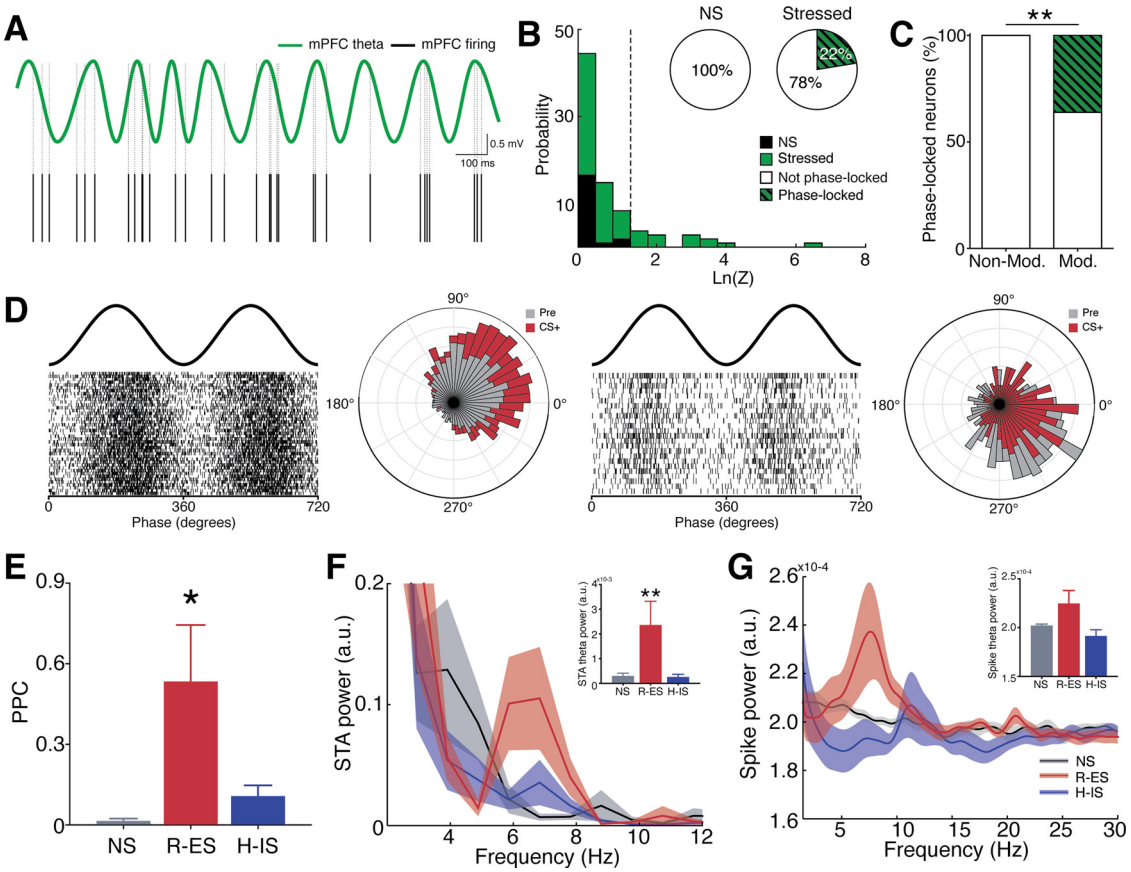

Figure 8. PFC neurons modulated under controllable stress are coupled with θ phase and rhythm. ***A***, Representative PFC θ-filtered signal with a neuron exhibiting phase-locked spikes. ***B***, Distribution of Rayleigh's Z parameter logarithm. Graded lines indicate the neurons considered significantly phase-locked. Pie charts show greater proportion of phase-locked neurons during stress (right) than NS (left). ***C***, Greater proportion of phase-locked neurons from modulated units compared with nonmodulated units. ***D***, Representative phase raster plots and polar histograms of two neurons from R-ES animals showing distinct modulations by CS^+ and strong θ phase-locking to different phases. ***E***, R-ES modulated neurons present stronger PPC. ***F***, Stronger spike-triggered averaged LFP θ power in R-ES modulated neurons. ***G***, Spike relative PSD showing prominent θ power in R-ES modulated neurons, indicating θ rhythmicity of these neurons. However, we found no statistical significance between averages.

presented a mean increase of θ power (PFC: 0.73 ± 0.14 dB; HPC: 0.62 ± 0.29 dB), H animals exhibited a decrease (PFC: -0.35 ± 0.20 dB; HPC: -0.66 ± 0.14 dB; Fig. 2*D–F*). Remarkably, R-ES and R-IS subgroups exhibited the same distinction against H-IS and H-ES (Fig. 3). In fact, we found that the behavioral outcome (R vs H) rather than the programmed stress exposure (ES vs IS) was the most significant factor influencing θ ERPP (two-way ANOVA, PFC: behavior $F_{(1,16)} = 13.01$, $p = 0.0024$; exposure $F_{(1,16)} = 1.68$, $p = 0.21$; HPC: behavior $F_{(1,16)} = 9.81$, $p = 0.0064$; exposure $F_{(1,16)} = 0.05$, $p = 0.81$; Fig. 3*C*,*D*). Furthermore, we found a negative correlation between θ ERPP on day 1 and latency to escape in the test session (day 3) across all stressed animals in both brain regions. This correlation was strong in the PFC ($r_{(18)} = -0.77$, $p < 0.0001$) and moderate in the HPC ($r_{(18)} = -0.58$, $p = 0.006$; Fig. 2*F*). In addition to confirming the strong correlations with escape performance, across the whole PFC spectrum, in the θ range (Fig. 2*G*), we observed that PFC θ ERPP was correlated to escape performance throughout the entire test session, while in the HPC, it was confined to the initial trials (Fig. 2*H*).

As we also noticed weaker correlations with behavior in other frequencies beyond θ, we investigated whether the whole-spectrum of PFC power modulations during stress could be collectively associated with resistance or helplessness through PCA. Surprisingly, the PC1 coefficients (Fig. 2*G*), which collectively account for the maximum data variance (35% explained variance; see inset of Fig. 2*G*), showed the same pattern as the spectrum of correlations with escape performance (Fig. 2*G*). Additionally, PC1 scores were significantly greater in R animals ($F_{(2,24)} = 12.57$, $p = 0.0002$; R vs H $t_{(24)} = 4.97$, $p < 0.0001$; R vs NS ($t_{(24)} = 2.68$, $p = 0.01$; H vs NS $t_{(24)} = 1.85$, $p = 0.07$), and they showed stronger correlation with subsequent escape latency ($r_{(18)} = -0.75$, $p = 0.0001$; Fig. 2*I*) than any frequency separately (Fig. 2*G*).

Aside from the relationship between θ and controllability, we observed that CS^+ profoundly decreased power in δ and α/β bands (1–30 Hz), regardless of the degree of control. We inspected the discrimination accuracy of all stressed animals (R plus H) against NS by the ERPP for each frequency and found the maximum distinction at the upper limits of β range (HPC: AUC = 0.99 at 24.04 Hz; PFC: AUC = 0.92 at 23.43 Hz; Fig. 3*C*,*D*, right panels). Also, the association between stimulus-triggered HPC θ power and stress control selectively occurred during CS^+ (theta power: two-way ANOVA period × stressor controllability interaction: $F_{(4,69)} = 2.21$, $p = 0.07$; CS *post hoc*: R vs. NS: $t_{(69)} = 3.50$, $p = 0.0008$; H vs. NS: $t_{(69)} = 0.14$, $p = 0.88$; R vs. H: $t_{(69)} = 3.78$, $p = 0.003$; θ power dB from pre-CS: two-way ANOVA period × stressor controllability interaction: $F_{(4,69)} = 2.63$, $p = 0.04$; CS *post hoc*: R vs H: $t_{(69)} = 4.17$, $p < 0.0001$; Fig. 4*A*,*B*), while the periods following the interruption of the USs (footshocks) were marked by transient increases in θ peak frequency, not power, regardless of their controllability (θ peak % from CS: two-way ANOVA period × stressor

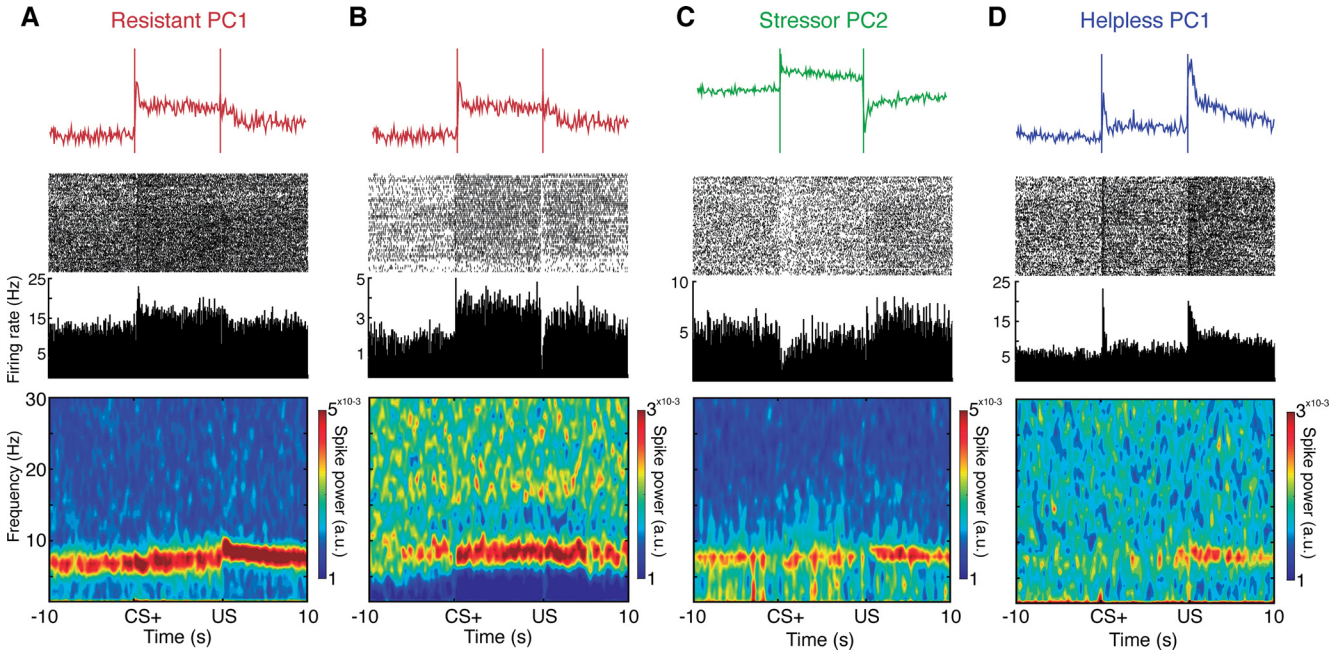

Figure 9. Representative neurons exhibiting the cooccurrence of stressor controllability-related firing patterns and θ rhythm. ***A–D***, Representative neurons displaying perievent firing rate responses (medium) consistent with the previously described patterns revealed through PCA (top), and evident spiking θ power (bottom). These neurons indicate that neuronal representations of stressor controllability are coupled with θ rhythm. ***A–C***, R-ES neurons consistent with (***A***, ***B***) resistant PC1 and (***C***) stressor PC2. Note the increases in spiking θ power parallel to decreases in firing rate after US. ***D***, H-IS neuron consistent with helpless PC1. Note the weaker spiking θ power during CS^+.

controllability interaction: $F_{(4,69)} = 19.44$, $p < 0.0001$; US *post hoc*: R vs NS: $t_{(66)} = 6.80$, $p < 0.0001$; H vs NS: $t_{(66)} = 6.63$, $p < 0.0001$; R vs H: $t_{(66)} = 0.09$, $p = 0.92$; theta power: US *post hoc*: R vs. NS: $t_{(69)} = 1.35$, $p = 0.18$; H vs. NS: $t_{(69)} = 0.92$, $p = 0.35$; R vs. H: $t_{(69)} = 0.43$, $p = 0.66$; θ power dB from pre-CS: US *post hoc*: R vs H: $t_{(69)} = 0.39$, $p = 0.69$; Fig. 4*C*). The elevations of HPC θ frequency after US (% from CS) were also shown to be a robust discriminator of stressed animals (AUC = 0.97). Although we found a suppression of PFC θ power during CS^+ associated with helplessness, H exhibited stronger θ phase resetting to CS^+ onset than NS (ITC ANOVA: $F_{(2,24)} = 2.27$, $p = 0.12$; *post hoc*: H vs NS: $t_{(24)} = 2.11$, $p = 0.04$; Fig. 4*D–G*).

Our results reveal an unprecedented association between both HPC and, especially, PFC θ power and stressor controllability. We found that the sustained engagement of θ power during the anticipation of aversive stimuli depends on the expectation of control and that this activity is related to the acquisition of long-term resistance to future stressors, as demonstrated by persistent active coping and the preserved ability of escape learning.

Enhanced HPC to PFC θ synchrony during stress correlates with learned resistance

To infer the functional connectivity between HPC and PFC, we calculated their phase coherence. The MPC spectra revealed an increase within the θ band during CS^+ in both R and H but not NS animals (Fig. 5*A*). This effect was observed to be consistent across all R and H subjects (Fig. 5*A*, insets) and MPC change to CS (% to pre-CS) revealed to be a robust discriminator of all stressed animals (AUC = 0.92). We also show that although θ MRL did not differ between groups during the pre-CS period, it was significantly modulated by both CS^+ and the expected degree of control (two-way ANOVA stressor controllability × period interaction $F_{(2,23)} = 21.85$, $p < 0.0001$; Fig. 5*B*). We found that θ MRL in both R and H were greater than NS ($t_{(46)} = 5.93$, $p < 0.0001$; $t_{(46)} = 2.76$, $p = 0.008$), and this effect was even greater in R than H ($t_{(46)} = 3.45$, $p = 0.001$; Fig. 5*B*). The directionality of θ LFP between regions was investigated through Granger causality analysis, which showed a prominent one-way directionality from the HPC to PFC in the θ range during CS^+ ($t_{(26)} = 3.55$, $p = 0.001$; Fig. 5*C*). We also examined the time delay between regions, and we showed that HPC θ signals constantly led the PFC by 49 ms during stress (maximum average cross-correlation: 49.00 ms; peak of lag distribution: 50.44 ± 3.56 ms; Fig. 5*D*,*E*). Moreover, we estimated time-frequency CS^+-related modulation of phase coherence, and we found a stronger HPC-PFC synchronization in R than H ($F_{(2,23)} = 12.03$, $p = 0.0003$; $t_{(23)} = 3.72$, $p = 0.001$; Fig. 5*F*,*G*). Also, similarly to the findings on θ power, we also observed that CS^+ θ MPC and its modulation were more associated with behavior than exposure (two-way ANOVA: MPC: behavior $F_{(1,16)} = 6.75$, $p = 0.01$; exposure $F_{(1,16)} = 0.28$, $p = 0.59$; normalized coherence: behavior ($F_{(1,16)} = 7.80$, $p = 0.01$; exposure $F_{(1,16)} = 0.09$, $p = 0.76$). Finally, HPC-PFC θ MPC during CS^+ was strongly correlated with the mean escape latency in the test session ($r_{(18)} = -0.70$, $p = 0.0005$; Fig. 5*H*). In addition to corroborating previous reports that HPC θ synchronizes with the PFC during the anticipation of aversive stimuli (Lesting et al., 2011), these results demonstrate that the strength of this synchronization is associated with controllability and learned resistance.

Prestimulus θ-γ phase-amplitude coupling in the PFC is associated with stress resistance and θ power modulation

The findings reported so far show that the network activity during CS^+ is highly associated with the expected degree of control over upcoming aversive stimuli. However, especially in the pre-CS period we observed a distinctively strong θ-γ phase-amplitude coupling (Fig. 6*A*) in R individuals. From the comodulation maps shown in Figure 6*B*, we observed that phase-amplitude coupling was specific to θ phases (4–10 Hz) and high γ (80–

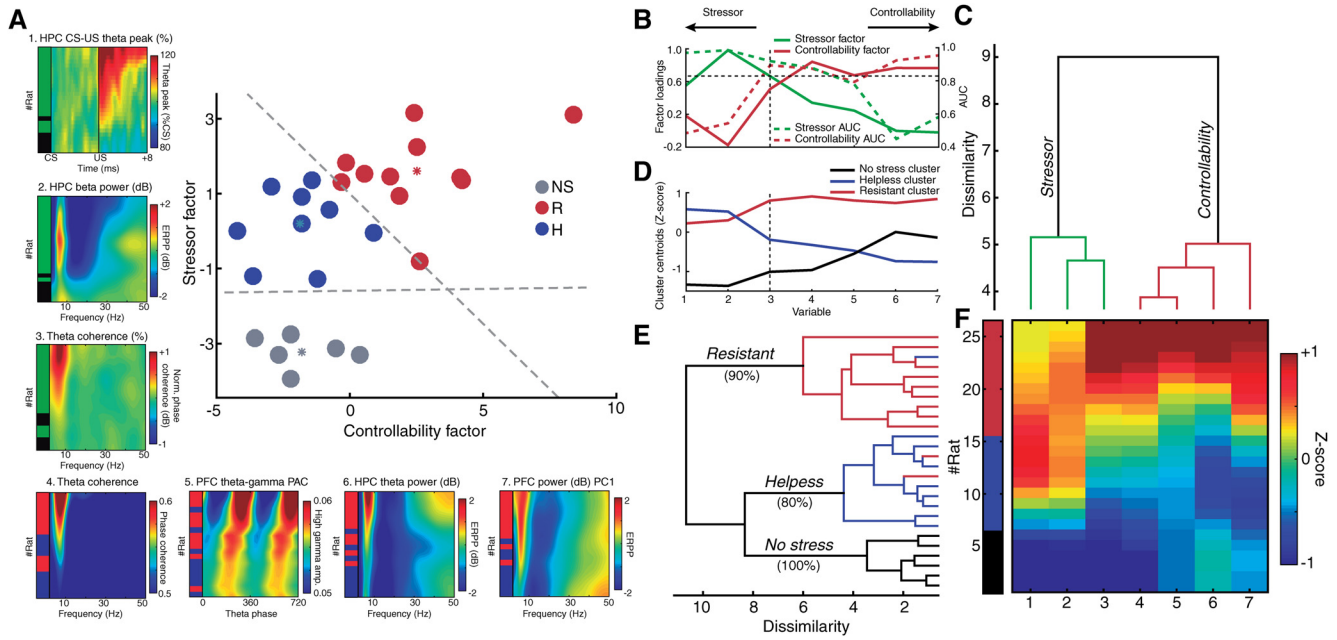

Figure 10. PFC and HPC network activities discriminate individuals under stress and predict resistance. ***A***, A linear model accurately discriminated individuals under stress and predicted resistance. ***A1–A7***, Electrophysiological variables used in the model: (1) change in US θ peak frequency (% from CS); (2) decrease in HPC β (24 Hz) power; (3) change in θ MPC (% from pre-CS); (4) θ MPC during CS; (5) PFC θ-high γ phase-amplitude coupling (MI); (6) HPC θ (7.7 Hz) power perturbation; (7) PFC spectral power perturbation PC1 score. The left bars indicate stressed (green) versus NS (black) individuals discriminated for variables 1–3, and R (red) versus H (blue) for variables 4–7. Dashed lines are the functions of the regularized linear discriminant classifier model. ***B***, Stressor and controllability are two dissociable factors influencing HPC-PFC network activity. Factor analysis for two factors returned factor loadings (solid lines) that weighted specifically on controllability-related variables (factor 1: controllability factor) or stressor-related variables (factor 2: stressor factor). Note the resemblance to the classification accuracy (AUC, dashed lines) of each variable for R versus H (red line) and S (stress group as the union of R and H) versus NS (green line). ***C***, Hierarchical clustering revealed that stressor-related (1–3) and controllability-related (4–7) variables were indeed dissociable. ***D***, ***E***, Hierarchical clustering revealed three distinctive clusters with specific (***D***) patterns of activity (cluster centroids) that (***E***) predominantly comprised individuals from each behavioral category. ***F***, Standardized values (smoothed Z-score) of each electrophysiological variable used in the model. Subjects were organized in NS, H, and R and were ordered by the sum of all effects.

110 Hz) amplitudes (Fig. 6*B*,*C*). PFC pre-CS MI was more effective in discriminating R from H individuals ($H_{(2)} = 7.92$, $p = 0.01$; R vs H: $U = 20$, $p = 0.04$; AUC = 0.77; Fig. 6*D*) than during the CS period (AUC = 0.61) and showed a significant association with behavior but not with exposure (two-way ANOVA: behavior $F_{(1,15)} = 5.00$, $p = 0.04$; exposure $F_{(1,15)} = 1.58$, $p = 0.22$). We excluded one R subject from these comparisons because of much higher PFC MI values than the other subjects. Conversely, HPC θ-high γ coupling was not associated with either stress or behavior (HPC pre-CS MI one-way ANOVA $F_{(2,23)} = 0.58$, $p = 0.56$; Fig. 6*E*). Consistently with previous studies (Tort et al., 2008), we found a correlation between θ-γ MI and θ power before CS^+ ($r_{s(17)} = 0.64$, $p = 0.002$), however, pre-CS MI was also correlated with CS^+ θ power ($r_{s(17)} = 0.64$, $p = 0.002$; Fig. 6*F*). Additionally, pre-CS MI also correlated with θ ERPP ($r_{s(17)} = 0.58$, $p = 0.007$; Fig. 6*G*). These findings indicate that basal θ-γ MI in the PFC is associated with stress resistance and controllability-related activity.

Differential neuronal firing responses to CS^+ and US is associated with controllability or helplessness

Previous studies have shown that PFC inhibition abolishes the protective effects of stressor controllability (Amat et al., 2005, 2006). Moreover, prelimbic neurons were reported to exhibit greater excitability *in vitro* after escapable but not inescapable stress (Varela et al., 2012). Maier and colleagues hypothesized that PFC activity would be excited under controllable stress, and either suppressed or not active under uncontrollable stress (Maier et al., 2006; Maier, 2015). We recorded PFC neuronal activity around ES and IS and we found no evidence for this hypothesis (Fig. 7). Furthermore, in contrast to our findings on network activities showing a clear distinction between R and H (Figs. 2, 3), we observed that neuronal activity was sensitive to both behavior (R vs H) and degree of control of the stress exposure (ES vs IS). Hence, we reasoned that the neural correlates of controllability and helplessness would be best represented in R-ES and H-IS neurons, so we focused on the latter groups for firing rate analyses. We analyzed the firing rates of spike-sorted neurons from NS ($N = 21$), R-ES ($N = 33$), H-ES ($N = 7$), R-IS ($N = 14$), and H-IS ($N = 35$; Fig. 7*A*). We observed a higher incidence of significantly stimulus-modulated neurons in stressed than NS animals [$\chi^2(1, N = 110) = 14.65$, $p = 0.0001$]. Differently from the hypothesis of PFC excitability under controllable stress, the proportions of excited or suppressed neurons did not differ between R-ES and H-IS, regardless of the trigger [CS^+: $\chi^2(2, N = 68) = 0.87$, $p = 0.64$; US: $\chi^2(2, N = 68) = 0.11$, $p = 0.94$; Fig. 7*B*]. Finally, we separately analyzed these subsamples of neurons, and found that excitation was actually enhanced in H-IS neurons, specifically after US termination ($F_{(2,35)} = 35.91$, $p < 0.0001$; R-ES vs H-IS $t_{(35)} = 4.34$, $p = 0.0001$; Fig. 7*C*,*D*).

Apart from the averaged patterns of Figure 7*C*,*D*, we observed a diversity of differential CS^+-evoked versus US-evoked firing modulations across individual neurons. Interestingly, this diversity was greater among stressed animals, suggesting that the differences between CS and US may be related to the encoding of stress-relevant information at the single-neuron level. To approach this question, we calculated the magnitude of US-evoked versus CS-evoked responses (i.e., the difference between their absolute values) across groups (Fig. 7*E*). This approach revealed an interesting marker of stress controllability ($F_{(2,54)} =$

3.02, $p = 0.056$, R-ES vs H-IS $t_{(54)} = 2.41$, $p = 0.019$): preferential neural reactivity to CS^+ in R-ES (-4.45 ± 2.95 Z-score) and to US in H-IS (3.70 ± 2.77 Z-score; Fig. 7*E*). Next, we characterized perievent patterns using PCA. The resistant PC1 (28% explained variance, $N = 47$) was characterized by a sustained increase in firing rate during CS^+, with a fast return to baseline after US. In contrast, the helpless PC1 (36% explained variance, $N = 42$) was rather characterized by phasic responses at CS^+ onset, but long-lived excitation at US offset (Fig. 7*G*). We then examined how well these perievent patterns would approximate those of CS^+-modulated or US-modulated neurons in R-ES versus H-IS. For this, correlations between PC1 coefficients and mean Z-scored firing rates of each neuron were converted to absolute values. We found that R-ES neurons showed greater correlation with the resistant PC1 ($H_{(2)} = 26.28$, $p < 0.0001$; R-ES vs H-IS $U = 97$, $p = 0.06$), and H-IS neurons with the helpless PC1 ($H_{(2)} = 27.04$, $p < 0.0001$; R-ES vs H-IS $U = 102$, $p = 0.09$; Fig. 7*G*). These findings demonstrate that PFC encoding of stressor controllability and uncontrollability are represented as complex perievent profiles around conditioned and unconditioned aversive stimuli. Our data also suggest an interdependence of these firing patterns on both the degree of control and the future behavior, strengthening a link between controllability, PFC activity, and acquisition of either resistance or helplessness.

PFC neurons modulated under controllable stress are coupled with θ phase and rhythm

Next, we investigated the interactions between single-neuron and oscillatory activities under controllable or uncontrollable stress. Initially, we observed that a proportion of neurons in stressed animals (22.80%, $N = 13/44$) showed significant phase-locked spiking to θ field potentials (Rayleigh's Z test, $p < 0.01$; see representative traces in Fig. 8*A*). In contrast, no phase-locked neurons were found in NS animals [0%, $N = 0/15$; $\chi^2(1, N = 72) = 4.17$, $p = 0.041$; Fig. 8*B*]. Additionally, all neurons that were phase-locked to θ LFP were also modulated by stress [phase-locked modulated 100%, $N = 13/13$; vs nonmodulated 52%, $N = 23/44$; $\chi^2(1, N = 57) = 9.82$, $p = 0.001$; Fig. 8*C*]. Then, we observed that modulated neurons in R-ES animals were more strongly phase-locked to PFC θ (representative units with both phase-locking and CS^+ responsivity are shown in Fig. 8*D*) than those of H-IS animals ($H_{(2)} = 13.19$, $p = 0.001$; R-ES vs H-IS $U = 39$, $p = 0.01$; Fig. 8*E*). We then investigated the possible association between LFP power and the spiking activity of neurons by estimating the PSDs of STA LFP. We found a prominent peak of STA θ power in R-ES modulated neurons ($H_{(2)} = 11.35$, $p = 0.003$; NS vs. R-ES $U = 24$, $p = 0.003$; R-ES vs. H-IS $U = 27$, $p = 0.002$ (Fig. 8*F*). We also explored spike rhythmicity itself by applying PSD analysis to the binary spiking data. This approach revealed stronger θ power among stimulus-modulated neurons of R-ES than NS or H-IS (Fig. 8*G*). Interestingly, some θ-rhythmic neurons also corresponded to the patterns of differential modulation by CS^+ versus US we described earlier: the resistant PC1 (greater to CS^+), the helpless PC1 (greater to US), and the stressor PC2 (opposed between CS^+ and US; Fig. 9, see also Fig. 7*F*). Altogether, our results suggest that θ rhythm coordinates the neuronal dynamics associated with stressor controllability and learned resistance within the PFC.

PFC and HPC network activities accurately discriminate individuals under stress and predict resistance to future uncontrollable stressors

Throughout this study, we reported a number of electrophysiological markers discriminating stressed from nonstressed animals (stressor-related variables), and R from H animals (controllability-related variables). We show that these variables are associated with distinct features of HPC-PFC θ oscillations, which in turn coordinate PFC neuronal firing patterns related to controllability. Our final approach was to explore patterns of activity that collectively comprise these variables and to examine how they could distinguish the effects of stress per se and predict resistance or helplessness.

The most relevant discriminators of stress and NS were: (1) elevation of HPC θ peak frequency after US (% from CS; AUC = 0.97; Fig. 4); (2) reduction of HPC β ERPP (maximum at 24.0 Hz; AUC = 0.99; Fig. 3); (3) HPC-PFC θ synchronization (AUC = 0.92; Figs. 5, 10*A1–A3*). In turn, the most relevant predictors of learned resistance and helplessness were: (4) HPC-PFC θ synchrony during CS^+ (AUC = 0.87; Fig. 5); (5) PFC prestimulus θ-γ MI (AUC = 0.79; Fig. 6); (6) increase in HPC θ ERPP (maximum at 7.7 Hz; AUC = 0.92; Figs. 2, 3); (7) PFC ERPP spectrum (2.5–50 Hz) PC1 score (AUC = 0.95; Figs. 2, 10*A*,*B*). We reasoned that we would be able to assemble the variables separately related to either stressor or controllability by computing factor analysis for two common factors (Fig. 10*A*,*B*). In fact, factor 1 loadings showed greater weights at controllability-related variables (>0.5), and lower weights at stressor-related variables (controllability factor; Fig. 10*B*). In turn, factor 2 loadings presented greater weights at stressor-related variables (> 0.5), and lowest weights at variables with bidirectional modulation by the degree of control (stressor factor; Fig. 10*B*). Consistently, the loadings of stressor and controllability factors resembled the univariate classification accuracies of each variable for stressed (vs NS) and R (vs H) subjects (Fig. 10*B*, dashed lines). Hierarchical clustering confirmed such distinction by showing that stressor-related and controllability-related variables are indeed dissociable (Fig. 10*C*). Thus, we obtained two scores representing the collective patterns of electrophysiological features related specifically to either controllability or stress per se.

Then we fitted a regularized linear discriminant classifier model based solely on these two predictors: stressor and controllability scores. Remarkably, our model reached 100% classification accuracy for all NS, R and H individuals simultaneously (100%, cross-validation: 92%, $N = 26$; Fig. 10*A*). Additionally, the model was also able to predict the behavioral outcomes of R-IS and H-ES animals (100%, $N = 6$), when fitted against NS, R-ES, and H-IS data ($N = 20$). Furthermore, we noticed that the arrangement of individuals revealed a striking characteristic. Although stressor scores were greater in both R and H animals compared with NS ($F_{(2,23)} = 52.49$, $p < 0.0001$; R vs NS $t_{(23)} = 10.21$, $p < 0.0001$; H vs NS $t_{(23)} = 6.93$, $p < 0.0001$; R vs H $t_{(23)} = 3.37$, $p = 0.002$), controllability scores were only significantly greater in R individuals ($F_{(2,23)} = 15.51$, $p < 0.0001$; R vs NS $t_{(23)} = 4.31$, $p = 0.0003$; R vs H $t_{(23)} = 4.95$, $p < 0.0001$), while H and NS were virtually identical (H vs NS $t_{(23)} = 0.06$, $p = 0.94$).

We also examined the presence of collective patterns of electrophysiological data across individuals through hierarchical clustering. This examination revealed three clearly distinct clusters fitting almost entirely the three behavioral categories of our study: R, H, and NS. Consistent with our model, the distinguishable patterns of activity (represented by cluster centroids, Fig. 10*D*) showed that the resistant cluster pattern was formed by the summation of stressor and controllability effects, while the helpless cluster pattern exhibited a clear resemblance to the stressor factor (Fig. 10*D*; see also Fig. 10*B*). This finding further illustrates that the neural activity underlying helplessness is essentially characterized by the effects of stress per se. Moreover, the

Table 1. Neural correlates of stressor, controllability, and uncontrollability

Variable	Stressor	Control	Uncontrol
HPC θ power*		↑	↓
HPC wide range power*	↓		
PFC θ power		↑	↓
PFC power perturbation PC1*		↑	↓
HPC θ peak frequency*	US>CS		
HPC-PFC synchrony**	↑	↑↑	
PFC θ phase resetting			↑
PFC θ-γ coupling*		↑	
PFC firing rate modulation	↑	CS>US	US>CS
PFC neuronal phase locking	↑	↑↑	

* variables used in the linear model, HPC = hippocampus, PFC = medial prefrontal cortex, CS = conditioned stimulus (light cue), US = unconditioned stimulus (footshock).

predominantly helpless cluster and the no stress cluster were clustered together in reference to the resistant cluster, which demonstrates that this latter group had the most distinctive activity (Fig. 10*E*). In fact, we identified the most distinctive collective pattern across subjects through PCA (48% explained variance, $N = 26$), and we observed that the PC1 scores showed the highest univariate prediction of R individuals (AUC = 0.98, $n = 11/26$), and the greatest correlation with escape performance reported in this study ($r_{(18)} = 0.77$, $p < 0.0001$; data not shown).

In summary, we found a clear dissociation between the effects of controllability and stress per se that defined the unique patterns of activity of nonstressed, R, and H individuals. Altogether, our findings converge to suggest that learned stressor resistance is associated with a distinctive collective pattern of enhanced HPC-PFC network θ activity during stress that is predominantly lacking in H individuals.

Discussion

Here, we performed the first electrophysiological investigation of animals during controllable or uncontrollable stress. We demonstrate that stressor controllability is associated with a distinctive pattern of enhanced hippocampal-prefrontal θ activity that predicts resistance against subsequent uncontrollable shocks, and that was predominantly absent in H individuals. The components of the controllability pattern and the stressor pattern are summarized in Table 1.

Unlike other animal models of depression based on natural individuals predispositions (Russo et al., 2012), the triadic design of learned helplessness models experiential factors that determine the outcomes of a stressful exposure. Our data link R-ES and H-IS to well-defined neural signatures, which can now be interpreted as correlates of the degrees of control over stress. Also interestingly, the neurophysiological profiles of the unforeseen minor subsamples R-IS and H-ES were consistent with their behavioral outcomes rather than their programmed stress exposure. We can attribute the incidence of R-IS to individual predispositions or accidental contingencies during the experiment (Skinner, 1948). In turn, the absence of the controllability signature in H-ES indicates that this activity is more linked to the "immunization" effect of behavioral control than to escape responses. In fact, PFC inhibition has been shown to spare escaping behavior, which is known to depend on subcortical structures (Canteras and Graeff, 2014), while abolishing the protective effects of controllability against subsequent induction of helplessness (Amat et al., 2005, 2006).

θ Functions and stressor controllability

Mounting evidence indicates that θ oscillations have a role in processing aversive information (Gray and McNaughton, 2000; Likhtik and Gordon, 2014; Bocchio et al., 2017; Çalışkan and Stork, 2019). Many reports describe increased θ power and synchrony during different stressors, including exposure to distant predators, aggressive conspecifics, anxiogenic environments, and conditioned fear (Sainsbury et al., 1987; Seidenbecher et al., 2003; Adhikari et al., 2010; Lesting et al., 2011; Hultman et al., 2018; Mikulovic et al., 2018). These observations suggest that θ oscillations may signal averseness and represent a correlate of fear and anxiety. In our study, we observed increases in θ power in R, but not H, animals. This finding is intriguing, given that helplessness is linked to exaggerated passive fear responses (Baratta et al., 2007). In this context, Courtin et al. (2014) reported suppression of PFC θ power during freezing, whereas Karalis et al. (2016) showed that abolishing θ activity does not alter freezing behavior. Although we observed CS^+-evoked θ synchronization in both R and H animals, which supports its role in signaling averseness, the strength of this synchrony was related to escape performance, which favors the role of θ activity in active coping. Adhikari et al. (2010) also reported that increased HPC-PFC θ synchrony in anxiogenic places predicts active avoidance toward safer zones. Causal evidence was recently provided by Padilla-Coreano et al. (2019), which showed that oscillatory optogenetic stimulation of the HPC-PFC pathway in the θ frequency promotes avoidance in the elevated plus maze. Also, Carlson et al. (2017) showed that θ-γ PFC stimulation promotes active struggling in the tail suspension test. Thus, high θ states during immobile fear behavior could be interpreted as the encoding of active responses, which is supported by the role of θ oscillations in sensorimotor integration and action selection (Oddie and Bland, 1998; Bender et al., 2015).

The differences in network dynamics related to stressor controllability were only observed during the CS^+ period. On the other hand, we found consistent US-induced increases of θ frequency regardless of controllability. This finding is consistent with reports showing that θ frequency increases with movement but persist for some time after the animal ceases it (McFarland et al., 1975), e.g., after high shock-avoidance jumps (Vanderwolf, 1969; Whishaw and Vanderwolf, 1973; Lenck-Santini et al., 2008) or pain-evoked behaviors (Khanna, 1997; Tai et al., 2006). Since we restricted our analyses to locomotion-free epochs, the neural signatures found during the anticipation of shocks may indeed represent correlates of distinct "expectations" of either controllability or uncontrollability.

Another finding reported here was the strong correlation of PFC θ power-synchrony during stress with later escape performance. In fact, extensive research has demonstrated that θ activity correlates with numerous forms of cognitive performance mostly related to memory encoding and retrieval, and executive functioning (Cavanagh and Frank, 2014; Hasselmo and Stern, 2014; Korotkova et al., 2018). Taken together, our results suggest that HPC-PFC θ activity supports cognitive mechanisms of stress resistance. In contrast, θ impairments in helplessness could mean that this syndrome stems from learning deficits rather than a learned response.

The intermediate HPC sends projections to the PFC and has been shown to participate in both cognitive and emotional functions (Fanselow and Dong, 2010). θ Oscillations are generated in the septal-hippocampal circuitry and synchronize with downstream targets on demand (Vertes and Kocsis, 1997; Buzsáki, 2002). Indeed, we observed that the HPC θ field entrained the PFC with a constant lag of 49 ms, consistently with previous reports (Siapas et al., 2005). However, we present evidence that

local PFC θ activity is important for stressor controllability. We observed a stronger correlation of PFC θ power with escape performance, and a unique association between stress resistance/controllability and PFC θ coupling to both fast oscillations and neuronal firing, which are known to be anatomically localized (Buzsáki et al., 2012). Thus, we conclude that the controllability pattern identified here represents an increased HPC-PFC network interaction that supports local processing in the PFC.

We report the surprising feature that differential firing to CS^+ and US possibly encode controllability-related information, and we evidence that these firing patterns are coordinated by θ rhythm. Prelimbic neurons have also been shown to signal averseness (Burgos-Robles et al., 2009; Sotres-Bayon and Quirk, 2010; Adhikari et al., 2011; Courtin et al., 2014; Diehl et al., 2018). Thus, we can interpret the immediate return to baseline firing after controllable US to represent the realization that averseness is no longer present. In contrast, the enduring responses after uncontrollable shocks in H animals would represent an impairment in such realization. It is worth mentioning that animals tend to generalize the expectations of either controllability or uncontrollability (Maier and Seligman, 1976), which makes it challenging to attribute single-neuron responses to distinct degrees of control. Nevertheless, our findings are sufficient to indicate that θ oscillations coordinate local PFC activity associated with the encoding of stressor controllability.

θ Impairment and helplessness

Our study suggests that helplessness might be associated with impaired θ engagement. This is consistent with reports that uncontrollable stress induces brain-wide serotonergic activation, which is the main modulatory system that suppresses θ (Vertes and Kocsis, 1997; Maier and Watkins, 1998; Puig and Gener, 2015). Serotonin-induced effects related to helplessness arise mostly from the dorsal raphe nucleus (Maier and Watkins, 2005), which receives regulatory projections from the PFC (Pollak Dorocic et al., 2014). This descending pathway has been consistently shown to mediate the protective effects of behavioral control (Warden et al., 2012; Maier, 2015). Furthermore, although there are no known projections from the HPC to the dorsal raphe nucleus, its neurons can be phase-locked to the θ field (Kocsis and Vertes, 1992; Pollak Dorocic et al., 2014). Thus, we speculate that θ influence on the dorsal raphe nucleus may be mediated via PFC, and that θ synchrony between these two regions may facilitate brain-wide stress-protective effects. Future studies should address these questions.

Maier and Seligman initially proposed that uncontrollability would be the key variable that, once learned, would change behavior (Seligman and Maier, 1967; Maier and Seligman, 1976). When PFC inhibition during controllable stress resulted in helplessness (Amat et al., 2005), the authors revisited the theory to suggest that actually controllability is the determining factor to be learned. In this sense, helplessness would develop as a default response to severe stress if controllability is absent (Maier and Seligman, 2016). We found that R and H individuals share electrophysiological markers of stress, but only R animals present the neural signature of controllability, in line with Maier and Seligman (Maier and Seligman, 2016).

Finally, our findings are in agreement with emerging treatment approaches for clinical depression. A recent meta-analysis concluded that frontal θ power was the electroencephalographic predictor of antidepressant response that was closest to proof of concept (Widge et al., 2019). Also, θ-burst transcranial magnetic stimulation of the PFC is a promising therapy against refractory depression (Cole et al., 2020). Here, we provide experimental evidence for a positive link between stress resilience and prefrontal θ, encouraging investigation of this activity as both a biomarker and a target in psychiatric treatments.

In conclusion, θ oscillations have been discussed to signal states of fear, anxiety, and stress vulnerability. By adding the controllability dimension to this scenario, we show that HPC-PFC θ activity may actually play a role in stress resistance. With our findings, we propose that the functions of hippocampal-prefrontal θ in stress, aversion, action selection, top-down regulation, learning, and cognitive control are integrated into a multidimensional continuum that underlies active coping against stressors.

References

Adhikari A, Topiwala MA, Gordon JA (2010) Synchronized activity between the ventral hippocampus and the medial prefrontal cortex during anxiety. Neuron 65:257–269.

Adhikari A, Topiwala MA, Gordon JA (2011) Single units in the medial prefrontal cortex with anxiety-related firing patterns are preferentially influenced by ventral hippocampal activity. Neuron 71:898–910.

Amat J, Matus-Amat P, Watkins LR, Maier SF (1998) Escapable and inescapable stress differentially and selectively alter extracellular levels of 5-HT in the ventral hippocampus and dorsal periaqueductal gray of the rat. Brain Res 797:12–22.

Amat J, Baratta MV, Paul E, Bland ST, Watkins LR, Maier SF (2005) Medial prefrontal cortex determines how stressor controllability affects behavior and dorsal raphe nucleus. Nat Neurosci 8:365–371.

Amat J, Paul E, Zarza C, Watkins LR, Maier SF (2006) Previous experience with behavioral control over stress blocks the behavioral and dorsal raphe nucleus activating effects of later uncontrollable stress: role of the ventral medial prefrontal cortex. J Neurosci 26:13264–13272.

Amat J, Aleksejev RM, Paul E, Watkins LR, Maier SF (2010) Behavioral control over shock blocks behavioral and neurochemical effects of later social defeat. Neuroscience 165:1031–1038.

Balleine BW, Curthoys IS (1991) Differential effects of escapable and inescapable footshock on hippocampal theta activity. Behav Neurosci 105:202–209.

Baratta MV, Christianson JP, Gomez DM, Zarza CM, Amat J, Masini CV, Watkins LR, Maier SF (2007) Controllable versus uncontrollable stressors bi-directionally modulate conditioned but not innate fear. Neuroscience 146:1495–1503.

Barnett L, Seth AK (2014) The MVGC multivariate Granger causality toolbox: a new approach to Granger-causal inference. J Neurosci Methods 223:50–68.

Bender F, Gorbati M, Cadavieco MC, Denisova N, Gao X, Holman C, Korotkova T, Ponomarenko A (2015) Theta oscillations regulate the speed of locomotion via a hippocampus to lateral septum pathway. Nat Commun 6:8521.

Berens P (2015) CircStat: a MATLAB toolbox for circular statistics. J Stat Softw 31:1–21.

Bocchio M, Nabavi S, Capogna M (2017) Synaptic plasticity, engrams, and network oscillations in amygdala circuits for storage and retrieval of emotional memories. Neuron 94:731–743.

Bueno-Junior LS, Simon NW, Wegener MA, Moghaddam B (2017) Repeated nicotine strengthens gamma oscillations in the prefrontal cortex and improves visual attention. Neuropsychopharmacology 42:1590–1598.

Bueno-Junior LS, Peixoto-Santos JE, Ruggiero RN, Ávila MAV, Marques DB, Lopes-Aguiar C, Leite JP (2018) Interaction between hippocampal-prefrontal plasticity and thalamic-prefrontal activity. Sci Rep 8:1382.

Burgos-Robles A, Vidal-Gonzalez I, Quirk GJ (2009) Sustained conditioned responses in prelimbic prefrontal neurons are correlated with fear expression and extinction failure. J Neurosci 29:8474–8482.

Buzsáki G (2002) Theta oscillations in the hippocampus. Neuron 33:325–340.

Buzsáki G, Draguhn A (2004) Neuronal oscillations in cortical networks. Science 304:1926–1929.

Buzsáki G, Anastassiou CA, Koch C (2012) The origin of extracellular fields and currents-EEG, ECoG, LFP and spikes. Nat Rev Neurosci 13:407–420.

Çalışkan G, Stork O (2019) Hippocampal network oscillations at the interplay between innate anxiety and learned fear. Psychopharmacology (Berl) 236:321–338.

Canteras NS, Graeff FG (2014) Executive and modulatory neural circuits of defensive reactions: implications for panic disorder. Neurosci Biobehav Rev 46:352–364.

Carlson D, David LK, Gallagher NM, Vu MAT, Shirley M, Hultman R, Wang J, Burrus C, McClung CA, Kumar S, Carin L, Mague SD, Dzirasa K (2017) Dynamically timed stimulation of corticolimbic circuitry activates a stress-compensatory pathway. Biol Psychiatry 82:904–913.

Cathomas F, Murrough JW, Nestler EJ, Han MH, Russo SJ (2019) Neurobiology of resilience: interface between mind and body. Biol Psychiatry 86:410–420.

Cavanagh JF, Frank MJ (2014) Frontal theta as a mechanism for cognitive control. Trends Cogn Sci 18:414–421.

Chapin JK, Nicolelis MAL (1999) Principal component analysis of neuronal ensemble activity reveals multidimensional somatosensory representations. J Neurosci Methods 94:121–140.

Cole EJ, Stimpson KH, Bentzley BS, Gulser M, Cherian K, Tischler C, Nejad R, Pankow H, Choi E, Aaron H, Espil FM, Pannu J, Xiao X, Duvio D, Solvason HB, Hawkins J, Guerra A, Jo B, Raj KS, Phillips AL, et al. (2020) Stanford accelerated intelligent neuromodulation therapy for treatment-resistant depression. Am J Psychiatry 177:716–726.

Courtin J, Chaudun F, Rozeske RR, Karalis N, Gonzalez-Campo C, Wurtz H, Abdi A, Baufreton J, Bienvenu TCM, Herry C (2014) Prefrontal parvalbumin interneurons shape neuronal activity to drive fear expression. Nature 505:92–96.

Diehl MM, Bravo-Rivera C, Rodriguez-Romaguera J, Pagan-Rivera PA, Burgos-Robles A, Roman-Ortiz C, Quirk GJ (2018) Active avoidance requires inhibitory signaling in the rodent prelimbic prefrontal cortex. Elife 7:e34657.

Fanselow MS, Dong HW (2010) Are the dorsal and ventral hippocampus functionally distinct structures? Neuron 65:7–19.

Feder A, Fred-Torres S, Southwick SM, Charney DS (2019) The biology of human resilience: opportunities for enhancing resilience across the life span. Biol Psychiatry 86:443–453.

Godsil BP, Kiss JP, Spedding M, Jay TM (2013) The hippocampal-prefrontal pathway: the weak link in psychiatric disorders? Eur Neuropsychopharmacol 23:1165–1181.

Gordon JA (2011) Oscillations and hippocampal-prefrontal synchrony. Curr Opin Neurobiol 21:486–491.

Grandchamp R, Delorme A (2011) Single-trial normalization for event-related spectral decomposition reduces sensitivity to noisy trials. Front Psychol 2:1–14.

Gray JA, McNaughton N (2000) The neuropsychology of anxiety: an enquiry into the function of the septo-hippocampal system. Oxford University Press, Oxford.

Hasselmo ME, Stern CE (2014) Theta rhythm and the encoding and retrieval of space and time. Neuroimage 85:656–666.

Hultman R, Ulrich K, Sachs BD, Blount C, Carlson DE, Ndubuizu N, Bagot RC, Parise EM, Vu MAT, Gallagher NM, Wang J, Silva AJ, Deisseroth K, Mague SD, Caron MG, Nestler EJ, Carin L, Dzirasa K (2018) Brain-wide electrical spatiotemporal dynamics encode depression vulnerability. Cell 173:166–180.e14.

Jay TM, Rocher C, Hotte M, Naudon L, Gurden H, Spedding M (2004) Plasticity at hippocampal to prefrontal cortex synapses is impaired by loss of dopamine and stress: importance for psychiatric diseases. Neurotox Res 6:233–244.

Joca SRL, Padovan CM, Guimarães FS (2003) Activation of post-synaptic 5-HT1A receptors in the dorsal hippocampus prevents learned helplessness development. Brain Res 978:177–184.

Kalisch R, Müller MB, Tüscher O (2015) A conceptual framework for the neurobiological study of resilience. Behav Brain Sci 38:e92.

Karalis N, Dejean C, Chaudun F, Khoder S, R, Rozeske R, Wurtz H, Bagur S, Benchenane K, Sirota A, Courtin J, Herry C (2016) 4-Hz oscillations synchronize prefrontal-amygdala circuits during fear behavior. Nat Neurosci 19:605–612.

Khanna S (1997) Dorsal hippocampus field CA1 pyramidal cell responses to a persistent versus an acute nociceptive stimulus and their septal modulation. Neuroscience 77:713–721.

Kim YC, Han SW, Alberico SL, Ruggiero RN, De Corte B, Chen KH, Narayanan NS (2017) Optogenetic stimulation of frontal D1 neurons compensates for impaired temporal control of action in dopamine-depleted mice. Curr Biol 27:39–47.

Kocsis B, Vertes RP (1992) Dorsal raphe neurons: synchronous discharge with the theta rhythm of the hippocampus in the freely behaving rat. J Neurophysiol 68:1463–1467.

Korotkova T, Ponomarenko A, Monaghan CK, Poulter SL, Cacucci F, Wills T, Hasselmo ME, Lever C (2018) Reconciling the different faces of hippocampal theta: the role of theta oscillations in cognitive, emotional and innate behaviors. Neurosci Biobehav Rev 85:65–80.

Lachaux JP, Rodriguez E, Martinerie J, Varela FJ (1999) Measuring phase synchrony in brain signals. Hum Brain Mapp 8:194–208.

Lenck-Santini PP, Fenton AA, Muller RU (2008) Discharge properties of hippocampal neurons during performance of a jump avoidance task. J Neurosci 28:6773–6786.

Lesting J, Narayanan RT, Kluge C, Sangha S, Seidenbecher T, Pape HC (2011) Patterns of coupled theta activity in amygdala-hippocampal-prefrontal cortical circuits during fear extinction. PLoS One 6:e21714.

Likhtik E, Gordon JA (2014) Circuits in sync: decoding theta communication in fear and safety. Neuropsychopharmacology 39:235–236.

Maier SF (2015) Behavioral control blunts reactions to contemporaneous and future adverse events: medial prefrontal cortex plasticity and a corticostriatal network. Neurobiol Stress 1:12–22.

Maier SF, Seligman MEP (1976) Learned helplessness: theory and evidence. J Exp Psychol 105:1–56.

Maier SF, Seligman MEP (2016) Learned helplessness at fifty: insights from neuroscience. Psychol Rev 123:1–19.

Maier SF, Watkins LR (1998) Stressor controllability, anxiety, and serotonin. Cognit Ther Res 22:595–613.

Maier SF, Watkins LR (2005) Stressor controllability and learned helplessness: the roles of the dorsal raphe nucleus, serotonin, and corticotropin-releasing factor. Neurosci Biobehav Rev 29:829–841.

Maier SF, Amat J, Baratta MV, Paul E, Watkins LR (2006) Behavioral control, the medial prefrontal cortex, and resilience. Dialogues Clin Neurosci 8:397–406.

McFarland WL, Teitelbaum H, Hedges EK (1975) Relationship between hippocampal theta activity and running speed in the rat. J Comp Physiol Psychol 88:324–328.

Mikulovic S, Restrepo CE, Siwani S, Bauer P, Pupe S, Tort ABL, Kullander K, Leão RN (2018) Ventral hippocampal OLM cells control type 2 theta oscillations and response to predator odor. Nat Commun 9:3638.

Narayanan NS, Laubach M (2009) Methods for studying functional interactions among neuronal populations. Methods Mol Biol 489:135–165.

Oddie SD, Bland BH (1998) Hippocampal formation theta activity and movement selection. Neurosci Biobehav Rev 22:221–231.

Oostenveld R, Fries P, Maris E, Schoffelen JM (2011) FieldTrip: open source software for advanced analysis of MEG, EEG, and invasive electrophysiological data. Comput Intell Neurosci 2011:156869.

Padilla-Coreano N, Canetta S, Mikofsky RM, Alway E, Passecker J, Myroshnychenko MV, Garcia-Garcia AL, Warren R, Teboul E, Blackman DR, Morton MP, Hupalo S, Tye KM, Kellendonk C, Kupferschmidt DA, Gordon JA (2019) Hippocampal-prefrontal theta transmission regulates avoidance behavior. Neuron 104:601–610.e4.

Pollak Dorocic I, Fürth D, Xuan Y, Johansson Y, Pozzi L, Silberberg G, Carlén M, Meletis K (2014) A whole-brain atlas of inputs to serotonergic neurons of the dorsal and median raphe nuclei. Neuron 83:663–678.

Pryce CR, Azzinnari D, Spinelli S, Seifritz E, Tegethoff M, Meinlschmidt G (2011) Helplessness: a systematic translational review of theory and evidence for its relevance to understanding and treating depression. Pharmacol Ther 132:242–267.

Puig MV, Gener T (2015) Serotonin modulation of prefronto-hippocampal rhythms in health and disease. ACS Chem Neurosci 6:1017–1025.

Rosenberg JR, Amjad AM, Breeze P, Brillinger DR, Halliday DM (1989) The Fourier approach to the identification of functional coupling between neuronal spike trains. Prog Biophys Mol Biol 53:1–31.

Royer S, Sirota A, Patel J, Buzsáki G (2010) Distinct representations and theta dynamics in dorsal and ventral hippocampus. J Neurosci 30:1777–1787.

Ruggiero RN, Rossignoli MT, Lopes-Aguiar C, Leite JP, Bueno-Junior LS, Romcy-Pereira RN (2018) Lithium modulates the muscarinic facilitation of synaptic plasticity and theta-gamma coupling in the hippocampal-prefrontal pathway. Exp Neurol 304:90–101.

Russo SJ, Murrough JW, Han M, Charney DS, Nestler EJ (2012) Neurobiology of resilience. Nat Neurosci 15:1475–1429.

Sainsbury RS, Heynen A, Montoya CP (1987) Behavioral correlates of hippocampal type 2 theta in the rat. Physiol Behav 39:513–519.

Seidenbecher T, Laxmi RT, Stork O, Pape HC (2003) Amygdalar and hippocampal theta rhythm synchronization during fear memory retrieval. Science 301:846–850.

Seligman MEP, Maier SF (1967) Failure to escape traumatic shock. J Exp Psychol 74:1–9.

Shors TJ, Seib TB, Levine S, Thompson RF (1989) Inescapable versus escapable shock modulates long-term potentiation in the rat hippocampus. Science 244:224–226.

Siapas AG, Lubenov EV, Wilson MA (2005) Prefrontal phase locking to hippocampal theta oscillations. Neuron 46:141–151.

Skinner BF (1948) Superstition in the pigeon. J Exp Psychol 38:168–172.

Sotres-Bayon F, Quirk GJ (2010) Prefrontal control of fear: more than just extinction. Curr Opin Neurobiol 20:231–235.

Southwick SM, Charney DS (2012) The science of resilience: implications for the prevention and treatment of depression. Science 338:79–82.

Tai SK, Huang FD, Moochhala S, Khanna S (2006) Hippocampal theta state in relation to formalin nociception. Pain 121:29–42.

Thierry AM, Gioanni Y, Dégénétais E, Glowinski J (2000) Hippocampo-prefrontal cortex pathway: anatomical and electrophysiological characteristics. Hippocampus 10:411–419.

Tort ABL, Kramer MA, Thorn C, Gibson DJ, Kubota Y, Graybiel AM, Kopell NJ (2008) Dynamic cross-frequency couplings of local field potential oscillations in rat striatum and hippocampus during performance of a T-maze task. Proc Natl Acad Sci USA 105:20517–20522.

Tort ABL, Komorowski RW, Manns JR, Kopell NJ, Eichenbaum H (2009) Theta-gamma coupling increases during the learning of item-context associations. Proc Natl Acad Sci USA 106:20942–20947.

Tort ABL, Komorowski R, Eichenbaum H, Kopell N (2010) Measuring phase-amplitude coupling between neuronal oscillations of different frequencies. J Neurophysiol 104:1195–1210.

Vanderwolf CH (1969) Hippocampal electrical activity and voluntary movement in the rat. Electroencephalogr Clin Neurophysiol 26:407–418.

Varela JA, Wang J, Christianson JP, Maier SF, Cooper DC (2012) Control over stress, but not stress per se increases prefrontal cortical pyramidal neuron excitability. J Neurosci 32:12848–12853.

Vertes RP, Kocsis B (1997) Brainstem-diencephalo-septohippocampal systems controlling the theta rhythm of the hippocampus. Neuroscience 81:893–926.

Vinck M, van Wingerden M, Womelsdorf T, Fries P, Pennartz CMA (2010) The pairwise phase consistency: a bias-free measure of rhythmic neuronal synchronization. Neuroimage 51:112–122.

Vollmayr B, Gass P (2013) Learned helplessness: unique features and translational value of a cognitive depression model. Cell Tissue Res 354:171–178.

Vollmayr B, Henn FA (2001) Learned helplessness in the rat: improvements in validity and reliability. Brain Res Brain Res Protoc 8:1–7.

Wang M, Perova Z, Arenkiel BR, Li B (2014) Synaptic modifications in the medial prefrontal cortex in susceptibility and resilience to stress. J Neurosci 34:7485–7492.

Warden MR, Selimbeyoglu A, Mirzabekov JJ, Lo M, Thompson KR, Kim SY, Adhikari A, Tye KM, Frank LM, Deisseroth K (2012) A prefrontal cortex-brainstem neuronal projection that controls response to behavioural challenge. Nature 492:428–432.

Whishaw IQ, Vanderwolf CH (1973) Hippocampal EEG and behavior: change in amplitude and frequency of RSA (theta rhythm) associated with spontaneous and learned movement patterns in rats and cats. Behav Biol 8:461–484.

Widge AS, Bilge MT, Montana R, Chang W, Rodriguez CI, Deckersbach T, Carpenter LL, Kalin NH, Nemeroff CB (2019) Electroencephalographic biomarkers for treatment response prediction in major depressive illness: a meta-analysis. Am J Psychiatry 176:44–56.

Willner P (1984) The validity of animal models of depression. Psychopharmacology (Berl) 83:1–16.

Wood J, Kim Y, Moghaddam B (2012) Disruption of prefrontal cortex large scale neuronal activity by different classes of psychotomimetic drugs. J Neurosci 32:3022–3031.

Yang Y, Cui Y, Sang K, Dong Y, Ni Z, Ma S, Hu H (2018) Ketamine blocks bursting in the lateral habenula to rapidly relieve depression. Nature 554:317–322.